# Diplomarbeit

# Cumulant Expansion Approach to Nonlinear Dynamics of Inhomogeneous Ensembles in Cavity QED

ausgeführt am

Institut für Theoretische Physik
der Technischen Universität Wien

———————————————

Institute for Theoretical Physics
Vienna University of Technology

unter der Anleitung von
Univ. Ass. Dr. rer. nat. Dmitry Krimer
und
Univ.-Prof. Dipl.-Ing. Dr. techn. Stefan Rotter,
durch

**Matthias Zens**
Reichental 105
2754 Waldegg
matthias.zens@gmail.com

| | |
|---|---|
| August 12, 2016 | |
| Datum | Unterschrift |

# Contents

# Abstract

In the last couple of years much effort has been dedicated to the development and the investigation of hybrid quantum devices, which combine the advantages of very dissimilar quantum systems for the realization of efficient quantum computation and communication technologies. Particularly interesting in this regard are solid-state quantum memories based on ensembles of spins (e.g. nitrogen vacancy defects in diamond or rare-earth doped crystals) coupled to superconducting microwave cavities. Here the spin-ensemble acts as a robust memory where the collective coupling to the cavity mode allows for the coherent transfer of quantum information. The major downside of ensembles inside solid-state systems is their natural tendency to exhibit inhomogeneous broadening of the transition frequencies, which makes experiments as well as their theoretical description very challenging. On the theoretical side it is primarily the computational complexity due to the exponential growth of the associated Hilbert space with the system size that inevitably calls for approximation schemes. To date, the theoretical description of large spin-cavity systems is mainly limited to weak driving fields, where the number of spin-excitations in the ensemble is negligible, corresponding to a Holstein-Primakoff approximation, or to mean-field approaches, where correlations within the system are neglected.

In this thesis we aim to develop a model that accurately accounts for the dynamics of large inhomogeneously broadened spin ensembles, coupled to a single cavity mode, even in the case of strong driving fields. In particular we employ the generalized cumulant expansion method to account for correlations within the system, which allows us to go beyond the Holstein-Primakoff and mean-field approximations. As a first step, we demonstrate the applicability of the cumulant expansion technique to the well-studied Jaynes-Cummings model and investigate its main limitations. We then move on to the Tavis-Cummings model with multiple spins inside the cavity and generalize our approach to ensembles containing a very large number of spins ($\sim 10^{12}$). Our model aims not only to provide a proper description of ensemble-based quantum memories, but also to serve as a novel tool for the investigation of interesting new physics arising from cooperative effects in inhomogeneous ensembles.

# Kurzzusammenfassung

In den vergangenen Jahren wurden große Anstrengungen in der Entwicklung und Untersuchung von hybriden Quantensystemen unternommen, welche die Vorteile von sehr unterschiedlichen Quantensystemen vereinen um damit Quantenrechner und Quanten-Kommunikationstechnologien effizient nutzbar zu machen. Von besonderem Interesse sind in diesem Zusammenhang Festkörper-Quantenspeicher basierend auf Spin-Ensembles (z.B. Stickstoff-Fehlstellen in Diamant oder mit Seltenen Erden dotierte Kristalle), gekoppelt an supraleitende Mikrowellen-Resonatoren. Dabei fungiert das Ensemble als robuster Speicher, wobei die kollektive Kopplung an die Resonator-Mode eine kohärente Übertragung von Quanteninformation ermöglicht. Der größte Nachteil von Spin-Ensembles in Festkörpersystemen ist ihre Tendenz zur inhomogenen Verbreiterung der Übergangsfrequenzen, was sowohl zu experimentellen wie auch zu theoretischen Herausforderungen führt. Letztere zeigen sich in Problemen der Berechenbarkeit aufgrund des exponentiellen Wachstums des Hilbert-Raums mit zunehmender Systemgröße, was Näherungsverfahren zwangsläufig erforderlich macht. Bislang ist die theoretische Beschreibung von großen gekoppelten Ensemble-Resonator-Systemen hauptsächlich beschränkt auf schwache Treibungsstärken, bei denen die Anzahl an Spin-Anregungen im Ensemble entsprechend einer Holstein-Primakoff-Näherung vernachlässigt werden kann, oder auf Mean-Field-Näherungen, welche Korrelationen innerhalb des Systems vernachlässigen.

In dieser Arbeit wollen wir ein Modell für die Dynamik von großen, inhomogen verbreiterten Spin-Ensembles gekoppelt an einen Resonator, entwickeln, das auch bei starker Treibung seine Gültigkeit behält. Wir verwenden dabei eine Entwicklungsmethode für verallgemeinerte Kumulanten, um Korrelationen im System berücksichten zu können, was eine wesentliche Verbesserung gegenüber der Holstein-Primakoff- und Mean-Field-Näherung darstellt. In einem ersten Schritt zeigen wir die Anwendbarkeit der Kumulanten-Entwicklungsmethode auf das gut untersuchte Jaynes-Cummings-Modell und untersuchen ihre Einschränkungen. Danach gehen wir über zum Tavis-Cummings-Modell mit mehreren Spins innerhalb des Resonators und verallgemeinern unseren Ansatz auf Ensembles die eine sehr große Anzahl an Spins ($\sim 10^{12}$) beinhalten. Unser Modell soll nicht nur eine korrekte Beschreibung von Ensemble-basierten Quantenspeichern zur Verfügung stellen, sondern auch als neuartiges Werkzeug zur Untersuchung von interessanter neuer Physik, resultierend aus kooperativen Effekten innerhalb inhomogener Ensemble, dienen.

# Chapter 1.

# Introduction

> *"Most phenomena we are familiar with involve such tremendous numbers of electrons that it's hard for our poor minds to follow that complexity. In such situations, we can use the theory to figure roughly what ought to happen and that is what happens, roughly, in those circumstances."*   -   *Richard P. Feynman* [1]

The theory of cavity quantum electrodynamics (QED), which deals with the interaction between matter and the quantized field modes in a resonator, was initiated already in 1946 by the pioneering work of Purcell [2]. Cavity QED soon moved into the spotlight as it opened up a new window on very fundamental issues of physics. Not only that the placement of an atom inside a cavity can enhance or likewise reduce its spontaneous emission rate [3, 4]; it is the atom-field coupling itself that is altered through the cavity, which thereby can give rise to a totally new behaviour of the coupled system. However, it was not until the 1980s that the so-called "strong coupling regime" was realized, where the coupling strength between the atoms and the field mode exceeds the total losses of the system, permitting the observation of self-induced Rabi oscillations [5]. The outstanding role of cavity QED arose not least from the development of an exactly solvable theoretical model for the interaction between an atom and a single mode of the quantized field, by Jaynes and Cummings [6]. This model, which now bears their names, stimulated the discovery of numerous remarkable properties and applications of coupled spin-cavity systems[1] [7–12].

*More Is Different*[2] - It is well known since the celebrated work by Dicke [14] that the simultaneous presence of many atoms, all interacting with the same electromagnetic field, can give rise to a cooperative behaviour of the system as a whole which is quite different from the superposition of effects arising from single atoms [15]. The investigation of such behaviour in the mean time became an actively developing area

---

[1] In its original version the model of Jaynes and Cummings comprised a molecule (two-level system) interacting with a single quantized cavity mode. Note that throughout this thesis we will use the terms *"spin"*, *"atom"*, and *"two-level system"* interchangeably, no matter if we are dealing with a real spin 1/2 or some other two-level system.

[2] Anderson (1972) [13]

of research on its own. In order to account for ensembles of atoms in cavity QED, Tavis and Cummings generalized the Jaynes-Cummings model to the case of many two-level systems [16]. The Tavis-Cummings model has gained renewed interest since the development and investigation of "hybrid quantum systems", which aim to combine the individual advantages of different quantum systems for novel quantum devices in the context of quantum computation and quantum communication technologies. Particularly attractive in this context are ensemble-based quantum memories coupled to superconducting microwave cavities [17–29]. Here the cavity serves as a quantum bus for the coherent in- and output of information which is to be stored in the ensemble. Among the most promising physical realizations are, for instance, negatively charged nitrogen vacancy defects in diamond [18–22], rare-earth doped crystals [23], clouds of ultracold atoms [24, 25] or magnons in yttrium iron garnet [26, 27]. The main drawback of most of these systems, however, is their natural inclination for inhomogeneous line broadening, which acts as the major source for decoherence. Besides the experimental difficulties that arise from the inhomogeneous broadening the theoretical ones are no less challenging. Clearly, the exponential growth of the Hilbert space with the number of constituent particles inevitably calls for approximation schemes.

*More Is Difficult* - Up to now, the theoretical description of large inhomogeneously broadened spin ensembles coupled to a cavity is mainly limited to the Holstein-Primakoff approximation [30], where the spin-dynamics is restricted to the south pole of the Bloch-sphere, or to semi-classical mean-field approaches. In particular, the Holstein-Primakoff approximation, which was successfully employed in previous studies [31–33], is limited to weak driving fields, where the number of photons inside the ensemble is always small as compared to the total number of spins. In this regime the number of excited spins can be readily neglected and the system behaves linearly with respect to the driving field amplitude. If the incident pulse, however, is increased to a certain value, the Holstein-Primakoff approximation breaks down and the system enters the nonlinear regime.

The goal of this thesis is to develop a theoretical model that goes beyond the Holstein-Primakoff approximation and mean-field methods such as to accurately describe the dynamics of an inhomogeneously broadened spin ensemble coupled to a single cavity mode even in the strong-driving regime. A common way to reduce the system size in many-particle configurations without restricting the excitation numbers is to truncate the correlations between the particles at some level. Such approaches are usually referred to as cluster-expansion methods [34, 35] and are used successfully in semiconductor quantum optics [36, 37]. In this thesis we develop a similar approach based on the generalized cumulant expansion [38] for the driven Jaynes-Cummings model, including inhomogeneously broadened ensembles and strong driving fields. With this theoretical framework we aim to provide a powerful instrument for the investigation of cooperative effects in the presence of inhomogeneous broadening. In particular our model will comprise complex collec-

tive phenomena like "superradiance" or its inverse counterpart "superabsorption" [14, 39]. Inhomogeneous broadening is expected to give rise to interesting new aspects of such nonlinear effects since it leads to important qualitative differences already on the linear level, as evidenced by the "cavity protection effect" [31, 32]. Hence the model we develop in this thesis constitutes not only an important tool for the theoretical description of certain hybrid quantum systems, but will also pave the way to study new fundamental effects that arise from inhomogeneous broadening in the nonlinear regime.

# Chapter 2.

# Model

In this chapter a theoretical model is developed to describe large and inhomogeneously broadened ensembles of two-level systems coupled to a single cavity mode in the presence of strong driving fields. The first section aims to provide a general introduction to the theoretical framework of our model. In the second section we focus on the actual implementation of these concepts for the driven Tavis-Cummings model. Finally, the last section deals with the clustering method developed to solve the resulting equations of motion even for very large ensembles.

## 2.1. Cumulant Expansion for Expectation Value Based Approaches

The following treatment covers the broad class of open quantum systems obeying the Markovian approximation with respect to their environment, which requires the correlation time between the system of investigation and its surrounding to be negligibly small[3]. The governing equation for open quantum systems of the Markovian type is the Lindblad master equation [41, 42]

$$\frac{d\rho}{dt} = -\frac{i}{\hbar}[H, \rho] + \mathcal{L} \,, \tag{2.1}$$

where the first term is the usual Liouville-von Neumann equation for a closed quantum system with the Hamiltonian $H$ and density operator $\rho$. The second term on the right hand side of Eq. (2.1) is the Lindblad term,

$$\mathcal{L} = \sum_m \frac{\lambda_m}{2} (2L_m \rho L_m^\dagger - L_m^\dagger L_m \rho - \rho L_m^\dagger L_m) \,, \tag{2.2}$$

which is responsible for the coupling to the environment. Here $\lambda_m$ and $L_m$ are the transition rates and jump operators respectively.

---

[3] A detailed description of the Markovian approximation can be found in any textbook on open quantum systems (see, e.g., [40, 41]).

Unfortunately, a direct solution of Eq. (2.1) is available only for very small systems, as the Hilbert space of a composite quantum system grows exponentially with the number of constituents. It is apparent that procedures which directly solve for the system's density matrix $\rho(t)$ quickly run into troubles for growing system sizes. However, in many cases it is not necessary to know the whole density matrix; in particular for correlated many-particle systems it is convenient to go immediately for the quantities of interest, such as expectation values, and derive equations of motion for them [34, 43–45].

**Hierarchy of Equations of Motion**    To obtain the equations of motion for the expectation value $\langle \hat{A} \rangle := Tr(\hat{A}\rho)$ of some operator $\hat{A}$, Eq. (2.1) is multiplied by $\hat{A}$. Following this, its trace is calculated;

$$Tr(\hat{A}\frac{d\rho}{dt}) = -\frac{i}{\hbar}Tr(\hat{A}[H,\rho]) + Tr(\hat{A}\mathcal{L})\,.$$

Using the time independence of the operator $\hat{A}$ in the Schrödinger picture, the commutativity of time derivative and trace operation as well as the cyclic permutability of the latter, one finally ends up with a generalized Ehrenfest equation of motion (cf. [34]),

$$\frac{d}{dt}\langle \hat{A} \rangle = -\frac{i}{\hbar}\langle [\hat{A}, H] \rangle + \sum_m \frac{\lambda_m}{2}\langle 2L_m^\dagger \hat{A} L_m - L_m^\dagger L_m \hat{A} - \hat{A}L_m^\dagger L_m \rangle\,. \qquad (2.3)$$

Performing this procedure, a hierarchy of linear differential equations is obtained. To stay on top of this set of equations, we sort them by the order of their expectation value. An expectation value of first-order in the following denotes the expectation value of a single operator only; a second-order expectation value denotes the joint expectation value of a product of two operators, and so on. The interaction part of $H$ couples the equations for $n$th-order expectation values to equations for expectation values of order $n+1$ and in this way generates an infinite hierarchy of coupled linear differential equations[4,5]

$$\frac{d}{dt}\langle 1 \rangle = \langle 1 \rangle + \langle 2 \rangle$$

$$\frac{d}{dt}\langle 2 \rangle = \langle 1 \rangle + \langle 2 \rangle + \langle 3 \rangle$$
$$\vdots$$
$$\frac{d}{dt}\langle n \rangle = \langle 1 \rangle + \langle 2 \rangle + \ldots + \langle n \rangle + \langle n+1 \rangle \qquad (2.4)$$
$$\vdots$$

---

[4] Such a hierarchy is usually called BBGKY hierarchy after Bogoljubow, Born, Green, Kirkwood, and Yvon [46].

[5] An explicit example, of such a hierarchical set of equations for a real physical system, is given in Appendix B.

Here $\langle n \rangle$ symbolizes some linear function of $n$th-order expectation values.

Solving any such system apparently requires a closed set of equations, and therefore demands truncation procedures. Equations (2.4) obviously form a closed set of equations, if $\langle n+1 \rangle = 0$ at some level. For small systems without gain such truncations come naturally, as the total number of excitations is limited and manageable. For instance, consider a system including one photon as single excitation; then all expectation values which contain two or more creation operators $a^\dagger$ vanish. As a result, the equations form a closed set, which can be readily solved [47]. Indeed, for such configurations usually the Lindblad master equation can be directly integrated as well, because the effective Hilbert space remains small. If the number of excitations is numerous instead, or depends on an external driving, different truncation strategies have to be used. In the following section such a truncation procedure, based on the generalized cumulant expansion, is developed.

## 2.1.1. Generalized Cumulants

Cumulants (or semi-invariants) play a very important role in probability theory as well as statistical physics[6], since they determine the character of the considered random variables [48, 49]. A brief repetition of the basic definitions of moments and cumulants for classical random variables can be found in Appendix A.

In his 1962 paper Kubo pioneered the significance of generalized cumulants for quantum mechanics [38]. Introducing an ordered exponential function and assuming that an average can be defined in such a way that it gives rise to a convergent moment generating function, the joint cumulant for operators $X_1, X_2, \ldots$ is defined as [38, 50]

$$\langle \mathcal{O}(X_1^{\alpha_1} X_2^{\alpha_2} \ldots) \rangle_c := \left[ \frac{\partial^{\alpha_1 + \alpha_2 + \ldots}}{\partial \xi_1^{\alpha_1} \partial \xi_2^{\alpha_2} \ldots} \ln \langle \mathcal{O}(e^{\xi_1 X_1 + \xi_2 X_2 + \ldots}) \rangle \right]_{\xi_i = 0} , \qquad (2.5)$$

where $\mathcal{O}$ is some ordering operator. Eq. (2.5) fully determines cumulants in terms of expectation values. The first-order cumulant of a certain operator $A$ corresponds to the expectation value $\langle A \rangle$ itself, whereas the second-order cumulant of two operators gives their covariance. The expressions for cumulants of higher order become more cumbersome. As an example, equations (2.6)-(2.9) show cumulants up to fourth order:

$$\langle A \rangle_c = \langle A \rangle \qquad (2.6)$$

$$\langle AB \rangle_c = \langle AB \rangle - \langle A \rangle \langle B \rangle \qquad (2.7)$$

$$\langle ABC \rangle_c = \langle ABC \rangle - \langle AB \rangle \langle C \rangle - \langle AC \rangle \langle B \rangle - \langle BC \rangle \langle A \rangle + 2 \langle A \rangle \langle B \rangle \langle C \rangle \qquad (2.8)$$

---

[6] In statistical physics the term Ursell function is more common.

$$\langle ABCD \rangle_c = \langle ABCD \rangle - \Big( \langle A \rangle \langle BCD \rangle + \langle B \rangle \langle ACD \rangle + \langle C \rangle \langle ABD \rangle \tag{2.9}$$

$$+ \langle D \rangle \langle ABC \rangle + \langle AB \rangle \langle CD \rangle + \langle AC \rangle \langle BD \rangle + \langle AD \rangle \langle BC \rangle \Big)$$

$$+ 2 \Big( \langle AB \rangle \langle C \rangle \langle D \rangle + \langle AC \rangle \langle B \rangle \langle D \rangle + \langle AD \rangle \langle B \rangle \langle C \rangle$$

$$+ \langle BC \rangle \langle A \rangle \langle D \rangle + \langle BD \rangle \langle A \rangle \langle C \rangle + \langle CD \rangle \langle A \rangle \langle B \rangle \Big)$$

$$- 6 \langle A \rangle \langle B \rangle \langle C \rangle \langle D \rangle$$

No simple formula for the expansion of high-order cumulants can be given. However, their calculation, using Eq. (2.5), is rather straightforward, although the resulting expressions become very cumbersome with increasing order. For the required truncation procedure we make use of two basic properties of cumulants:

(i) A cumulant of certain order can be solely expressed by expectation values of the same and lower order.

(ii) If one or more operators are statistically independent from the others, the corresponding cumulant equals zero. In other words, cumulants of statistically unconnected operators vanish.

## 2.1.2. Truncation Procedure

Employing the latter property (ii) of cumulants from above, truncating cumulants for many physical systems comes more naturally than the truncation of expectation values mentioned earlier. Even if the number of excitations is numerous, one can assume that contributions from cumulants of rising order decrease, as do the correlations between increasing numbers of constituents. Therefore (instead of setting $\langle n + 1 \rangle = 0$ ) it is assumed that at a certain order

$$\langle n + 1 \rangle_c \approx 0 \,. \tag{2.10}$$

It then follows through property (i) that the expectation values of the $(n+1)$-th order can be well approximated by a nonlinear combination of lower-order expectation values

$$\langle n + 1 \rangle \approx f\big( \langle n \rangle, \langle n - 1 \rangle, \ldots, \langle 1 \rangle \big) \,, \tag{2.11}$$

which allows to truncate the hierarchy of equations (2.4) to obtain a closed set of equations, as illustrated in Figure (2.1),

$$\frac{d}{dt} \langle 1 \rangle = \langle 1 \rangle + \langle 2 \rangle$$

$$\frac{d}{dt} \langle 2 \rangle = \langle 1 \rangle + \langle 2 \rangle + \langle 3 \rangle \tag{2.12}$$

$$\vdots$$

$$\frac{d}{dt} \langle n \rangle = \langle 1 \rangle + \langle 2 \rangle + \ldots + \langle n \rangle + f\big( \langle n \rangle, \langle n - 1 \rangle, \ldots, \langle 1 \rangle \big) \,.$$

Here $f\big(\langle n\rangle, \langle n-1\rangle, \ldots, \langle 1\rangle\big)$ is some nonlinear function involving solely expectation values of order $n$ and lower. Thus, the infinite hierarchy of linear differential equations (2.4) turns into a closed set of nonlinear differential equations (2.12), where the nonlinearities arise from the truncation (2.11). The explicit form of the nonlinear function $f\big(\langle n\rangle, \ldots, \langle 1\rangle\big)$ for the first three orders can be inferred from the equations (2.7)-(2.9):

$$\langle AB\rangle \approx \langle A\rangle\langle B\rangle \tag{2.13}$$

$$\langle ABC\rangle \approx \langle AB\rangle\langle C\rangle + \langle AC\rangle\langle B\rangle + \langle BC\rangle\langle A\rangle - 2\langle A\rangle\langle B\rangle\langle C\rangle \tag{2.14}$$

$$\begin{aligned}
\langle ABCD\rangle \approx{}& \langle A\rangle\langle BCD\rangle + \langle B\rangle\langle ACD\rangle + \langle C\rangle\langle ABD\rangle + \langle D\rangle\langle ABC\rangle \\
&+ \langle AB\rangle\langle CD\rangle + \langle AC\rangle\langle BD\rangle + \langle AD\rangle\langle BC\rangle \\
&- 2\Big(\langle AB\rangle\langle C\rangle\langle D\rangle + \langle AC\rangle\langle B\rangle\langle D\rangle + \langle AD\rangle\langle B\rangle\langle C\rangle \\
&\quad + \langle BC\rangle\langle A\rangle\langle D\rangle + \langle BD\rangle\langle A\rangle\langle C\rangle + \langle CD\rangle\langle A\rangle\langle B\rangle\Big) \\
&+ 6\langle A\rangle\langle B\rangle\langle C\rangle\langle D\rangle
\end{aligned} \tag{2.15}$$

From now on, we denote the truncation of all second-order expectation values, $\langle AB\rangle \approx \langle A\rangle\langle B\rangle$, as the first-order cumulant expansion. Eqs. (2.14) and (2.15) then correspond to the second-, and third-order cumulant expansion, respectively. Note that, by property (ii), the approximations (2.13)-(2.15) are exact, if one of the operators is statistically independent of the others.

**Intuitive Approach to the Cumulant Expansion**  Before we move on to a concrete application of the cumulant expansion, we aim to complement to the subject an intuitive approach that was developed during this thesis. Instead of starting from the pure mathematical definition Eq. (2.5) it is instructive to begin our investigation from the latter property (ii) of cumulants, which allows for a more physical motivation. It follows right from statistical independence that the relation $\langle AB\rangle = \langle A\rangle\langle B\rangle$ holds, if $A$ and $B$ are statistically unconnected [51]. In order to truncate the hierarchic set of equations (2.4) at higher orders, we seek for a generalization of this factorization for expectation values involving more than two operators. We therefore make the general ansatz

$$\langle ABC\rangle = \alpha\langle AB\rangle\langle C\rangle + \beta\langle AC\rangle\langle B\rangle + \gamma\langle BC\rangle\langle A\rangle + \delta\langle A\rangle\langle B\rangle\langle C\rangle\,, \tag{2.16}$$

with unknown coefficients $\alpha$, $\beta$, $\gamma$, and $\delta \in \mathbb{R}$. Indeed, this ansatz should comprise the extreme cases where a single or all operators are statistically unconnected. Let

us consider, as an example, that the operator $A$ is statistically independent of the other two operators $B$ and $C$; then clearly the relation

$$\langle \underline{A}BC \rangle = \langle \underline{A} \rangle \langle BC \rangle \tag{2.17}$$

holds, where the underline ("_") indicates the statistical independence of $A$. The ansatz (2.16) simplifies to

$$
\begin{aligned}
\langle \underline{A}BC \rangle &= \alpha \langle \underline{A}B \rangle \langle C \rangle + \beta \langle \underline{A}C \rangle \langle B \rangle + \gamma \langle BC \rangle \langle \underline{A} \rangle + \delta \langle \underline{A} \rangle \langle B \rangle \langle C \rangle \\
&= \alpha \langle \underline{A} \rangle \langle B \rangle \langle C \rangle + \beta \langle \underline{A} \rangle \langle C \rangle \langle B \rangle + \gamma \langle BC \rangle \langle \underline{A} \rangle + \delta \langle \underline{A} \rangle \langle B \rangle \langle C \rangle \\
&= \gamma \langle \underline{A} \rangle \langle BC \rangle + (\alpha + \beta + \delta) \langle \underline{A} \rangle \langle B \rangle \langle C \rangle \, .
\end{aligned}
\tag{2.18}
$$

A coefficient comparison of (2.17) and (2.18) gives the relations

$$\gamma = 1 \qquad \text{and} \qquad \alpha + \beta + \delta = 0 \, . \tag{2.19}$$

The same argument applies to statistically independent operators $\underline{B}$ and $\underline{C}$ which gives $\beta = 1$ and $\alpha = 1$, respectively. Hence, the coefficients in Eq. (2.16) are determined:

$$\alpha = \beta = \gamma = 1 \, , \quad \delta = -2 \, . \tag{2.20}$$

Obviously, our intuitive approach coincides with the expansion (2.14), which was obtained using Eq. (2.5). A similar calculation can be made to derive the third-order cumulant expansion (2.15); however, we will not show it here but move on to the application of the cumulant expansion to the driven Tavis-Cummings model.
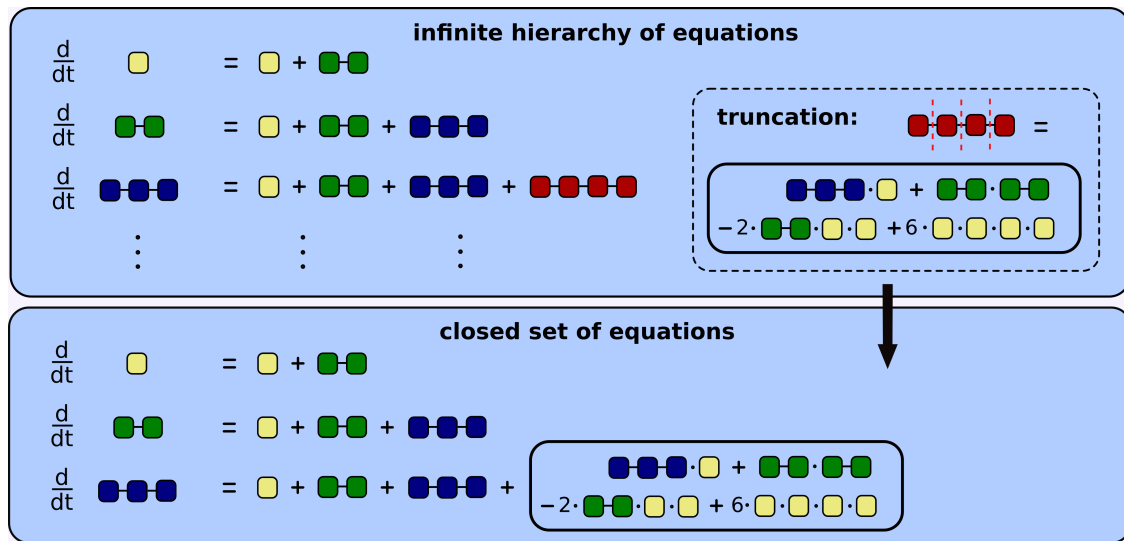
Figure 2.1.: Pictogram of the cumulant expansion method. 1st-order expectation values are represented by single unconnected squares (*yellow*); 2nd-, 3rd-, and 4th-order expectation values are represented by two (*green*), three (*blue*), and four (*red*) connected squares, respectively. The truncation is indicated by *dashed red lines* cutting the connections (*solid black lines*) between individual squares.

## 2.2. Tavis-Cummings Model with External Driving

In this section we apply the cumulant expansion technique described above to the interesting case of an inhomogeneously broadened ensemble of two-level systems coupled to a single cavity mode, as illustrated in Figure 2.2. Our approach includes dissipation to the environment through cavity and spin losses as well as a coherent external driving field using the input-output formalism of Gardiner and Collett [52]. Physical realizations of this model can include, for instance, negatively charged nitrogen vacancy defects in diamond [18–20, 22], rare-earth spin ensembles [23], clouds of ultracold atoms [24, 25] or magnons in yttrium iron garnet [26, 27].
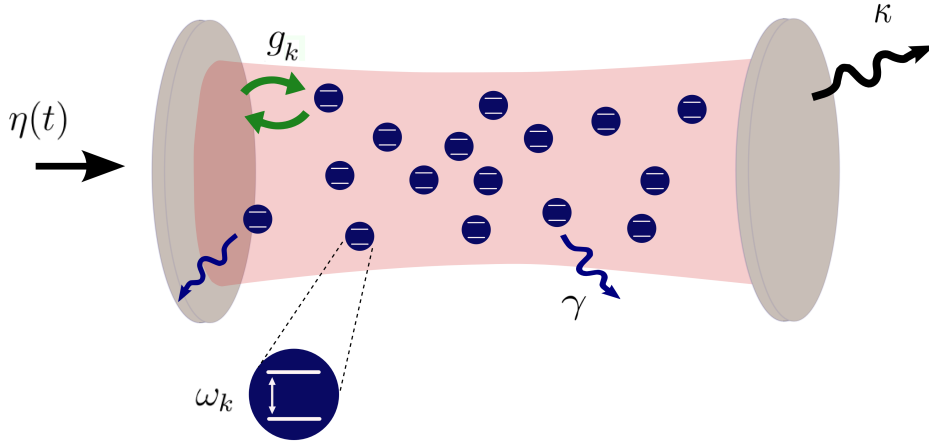


Figure 2.2.: Schematic of the physical system under investigation. An ensemble of two-level systems (*blue spots*) is coupled to a single cavity mode (*reddish area*) with the individual coupling strength $g_k$ (*green arrows*). The system is driven by an external field $\eta$ and involves dissipation to the environment through cavity and spin losses, $\kappa$ and $\gamma$.

**Tavis-Cummings Hamiltonian**    On the one hand, we consider a spin ensemble which is well confined inside the cavity, so that all two-level systems experience the same electric field. The spatial density of the ensemble, on the other hand, is assumed to be sparse, to guarantee that dipole-dipole interaction among individual spins can be neglected. Under these assumptions the system under consideration is well described by the Tavis-Cummings Hamiltonian ($\hbar = 1$) [16]

$$H = \omega_c a^\dagger a + \frac{1}{2} \sum_{k=1}^{N} \omega_k \sigma_k^z + \sum_{k=1}^{N} \left( g_k \sigma_k^- a^\dagger + g_k^* \sigma_k^+ a \right)$$

$$+ i \left( \eta \, a^\dagger e^{-i\omega_p t} - \eta^* a \, e^{i\omega_p t} \right), \tag{2.21}$$

where $a^\dagger, a$ are the standard creation and annihilation operators of the cavity field; $\sigma_k^z, \sigma_k^\pm$ are the Pauli operators of the $k$-th spin and $N$ is the total number of spins in the ensemble. The first two terms, hence, correspond to the energy of the uncoupled cavity mode with frequency $\omega_c$ and the ensemble of two-level systems with transition frequencies $\omega_k$, respectively. The third term accounts for the interaction between the cavity field and the spin ensemble, written in the rotating wave approximation (where the terms proportional to $\sigma_k^- a$ and $\sigma_k^+ a^\dagger$ are neglected); here $g_k$ is the individual coupling strength of the $k$-th spin to the cavity mode. Finally, the last term acts as an external driving field of amplitude $\eta$ and frequency $\omega_p$ [53, p.276].

**Lindblad Term**  To account for losses of the system we have to specify the Lindblad term of the master equation (2.1). For our model we consider interactions with the environment of the form [19]:

$$
\begin{aligned}
\mathcal{L}(\rho) = \kappa \left(2a\rho a^\dagger - a^\dagger a\,\rho - \rho\,a^\dagger a\right) &\qquad \rightarrow \quad \text{cavity-bath} \\[2ex]
+ \gamma_h \sum_{k=1}^{N} (2\sigma_k^- \rho\,\sigma_k^+ - \sigma_k^+ \sigma_k^- \rho - \rho\,\sigma_k^+ \sigma_k^-) &\qquad \rightarrow \quad \text{ensemble-bath} \\[2ex]
+ \gamma_p \sum_{k=1}^{N} (\sigma_k^z \rho\,\sigma_k^z - \rho)\,, &\qquad \rightarrow \quad \text{non-radiative dephasing}
\end{aligned}
\tag{2.22}
$$

where the first term corresponds to the cavity losses of rate $\kappa$; the second term gives the radiative decay of the individual spins at rate $\gamma_h$, and the last term describes their non-radiative dephasing by introducing the decay rate $\gamma_p/2$ [40]. Notice that the latter term is still of the Lindblad type (2.2), using the identity $\sigma_k^z \sigma_k^z = \hat{1}$. Further note that in (2.22) we neglect thermal fluctuations, which are negligible for $k_B T \ll \hbar \omega_k$.

The Tavis-Cummings Hamiltonian (2.21), along with the Lindblad term (2.22), fully determines the behaviour of the system through the Lindblad master equation (2.1), $d\rho/dt = -i[H, \rho] + \mathcal{L}$. In order to solve the dynamics of this problem, we follow the procedure presented in Section (2.1) and derive equations of motion for the expectation values of the operators for the cavity mode and the spin degrees of freedom. Using the commutation relations[7]

$$
[a, a^\dagger] = \hat{1}\,, \qquad [\sigma_k^+, \sigma_j^-] = \sigma_k^z \delta_{kj}\,, \qquad [\sigma_k^z, \sigma_j^\pm] = \pm 2\sigma_k^\pm \delta_{kj}\,, \tag{2.23}
$$

---

[7] Here $\sigma^z$ and $\sigma^\pm$ are the Pauli operators $\sigma^z := \begin{pmatrix} 1 & 0 \\ 0 & -1 \end{pmatrix}$, $\sigma^+ := \frac{1}{2}(\sigma^x + i\sigma^y) = \begin{pmatrix} 0 & 1 \\ 0 & 0 \end{pmatrix}$, and $\sigma^- := \frac{1}{2}(\sigma^x - i\sigma^y) = \begin{pmatrix} 0 & 0 \\ 1 & 0 \end{pmatrix}$ in contrast to the spin operators $S^z := \frac{1}{2}\sigma^z$ and $S^\pm := \sigma^\pm$, which give rise to slightly different commutation relations.

we obtain a hierarchic set of coupled differential equations that is shown up to third order in Appendix B and serves as starting point for all further investigations. For reasons of clarity and comprehensibility, we present here only the first-order equations,

$$\frac{d}{dt}\langle a\rangle = -(\kappa + i\,\Delta_c)\,\langle a\rangle - i\sum_{k=1}^{N} g_k\,\langle\sigma_k^-\rangle + \eta\,, \tag{2.24}$$

$$\frac{d}{dt}\langle\sigma_k^-\rangle = -(\gamma_h + 2\gamma_p + i\,\Delta_k)\,\langle\sigma_k^-\rangle + i\,g_k\,\langle\sigma_k^z a\rangle\,, \tag{2.25}$$

$$\frac{d}{dt}\langle\sigma_k^z\rangle = -2\gamma_h(\langle\sigma_k^z\rangle + 1) - 4\,g_k\,\mathrm{Im}(\langle\sigma_k^- a^\dagger\rangle)\,, \tag{2.26}$$

where we introduced $\Delta_c := \omega_c - \omega_p$ and $\Delta_k := \omega_k - \omega_p$. For simplicity, we choose in our calculations the coupling strengths $g_k$ and the amplitude of the driving field $\eta$ to be real valued.

In the following sections we truncate the hierarchy of equations (B.1)-(B.25) employing two different methods. First, we introduce the Holstein-Primakoff approximation [30], which can be effectively applied in the linear regime at weak driving fields [31–33]. Following this, we utilize the cumulant expansion method, developed above, to account also for nonlinear behaviour of the system at stronger driving fields.

## 2.2.1. Holstein-Primakoff Approximation

For weak driving fields $\eta(t)$ the dynamics of large ensembles can be calculated very accurately assuming that most spins remain unexcited, $\langle\sigma_k^z\rangle \approx -1$, which is the so-called Holstein-Primakoff approximation. Under this assumption, the term "$\langle\sigma_k^z a\rangle$" in Equation (2.25) can be replaced by "$-\langle a\rangle$". As a result, (2.24) and (2.25) form a closed set of equations by themselves:

$$\frac{d}{dt}\langle a\rangle = -(\kappa + i\,\Delta_c)\,\langle a\rangle - i\sum_{k=1}^{N} g_k\,\langle\sigma_k^-\rangle + \eta \tag{2.27}$$

$$\frac{d}{dt}\langle\sigma_k^-\rangle = -(\gamma_h + 2\gamma_p + i\,\Delta_k)\,\langle\sigma_k^-\rangle - i\,g_k\,\langle a\rangle\,, \tag{2.28}$$

which can be solved efficiently for large ensembles by going to the continuous limit and setting up a Volterra integral equation [32]. The coupled equations (2.27) and (2.28), however, are completely linear, and therefore do not describe any nonlinear physical effects, such as optical bistability [15]. Clearly, if we turn to strong driving fields, the number of spin-excitations can not be neglected and the Holstein-Primakoff approximation fails.

## 2.2.2. Cumulant Expansion Method

Since the Holstein-Primakoff approximation disregards the number of excited spins, it misses to account for any nonlinear effects regarding $\eta(t)$. In this section we overcome this drawback by invoking the cumulant expansion method, which inevitably results in a nonlinear theory. We start with the first-order cumulant expansion, which corresponds to a mean-field approach and can be understood from a very intuitive point of view. Then we move on to the more sophisticated second- and third-order cumulant expansion method, using the truncation procedures (2.14) and (2.15).

**First-Order Cumulant Expansion**    The most simple approach to the system dynamics in case of considerable spin excitations is accomplished by factorising the expectation values $\langle \sigma_k^z a \rangle$ and $\langle \sigma_k^- a^\dagger \rangle$ into $\langle \sigma_k^z \rangle \langle a \rangle$ and $\langle \sigma_k^- \rangle \langle a \rangle^*$, respectively. Equations (2.24) - (2.26) then become

$$\frac{d}{dt}\langle a \rangle = -(\kappa + i\,\Delta_c)\,\langle a \rangle - i\sum_{k=1}^{N} g_k\,\langle \sigma_k^- \rangle + \eta\,, \tag{2.29}$$

$$\frac{d}{dt}\langle \sigma_k^- \rangle = -(\gamma_h + 2\gamma_p + i\,\Delta_k)\,\langle \sigma_k^- \rangle + i\,g_k\,\langle \sigma_k^z \rangle\,\langle a \rangle \,, \tag{2.30}$$

$$\frac{d}{dt}\langle \sigma_k^z \rangle = -2\gamma_h(\langle \sigma_k^z \rangle + 1) - 4\,g_k\,\mathrm{Im}(\langle \sigma_k^- \rangle\,\langle a \rangle^*)\,, \tag{2.31}$$

which is a closed set of nonlinear differential equations, which can be solved at least numerically. It is apparent from Eq. (2.7) that the complete factorizations

$$\langle \sigma_k^z a \rangle = \langle \sigma_k^z \rangle\,\langle a \rangle \quad \text{and} \quad \langle \sigma_k^- a^\dagger \rangle = \langle \sigma_k^- \rangle\,\langle a \rangle^* \tag{2.32}$$

imply that all correlations within the system are omitted

$$\langle \sigma_k^z a \rangle_c = \langle \sigma_k^- a^\dagger \rangle_c = 0\,, \tag{2.33}$$

corresponding to a mean-field theory [45]. Clearly, such cumulants gain significance for an increasing driving field $\eta(t)$, since the photons mediate an indirect spin-spin interaction and thereby give rise to the formation of correlations within the system. On our route towards a reliable method for calculating the system dynamics at strong driving fields, we therefore follow the strategy to include higher orders of cumulants in our model.

**Second-Order Cumulant Expansion**   To account for correlations within the system it is necessary to invoke at least second-order expectation values. Equations (B.1) - (B.12) constitute the basis of the second-order cumulant expansion; they include equations of motion for all expectation values up to second-order, which are 12 in total: $\langle a \rangle$, $\langle \sigma_k^- \rangle$, $\langle \sigma_k^z \rangle$, $\langle \sigma_k^z a \rangle$, $\langle \sigma_k^z \sigma_j^- \rangle$, $\langle \sigma_k^- a^\dagger \rangle$, $\langle \sigma_k^+ \sigma_j^- \rangle$, $\langle \sigma_k^- a \rangle$, $\langle a^\dagger a^\dagger \rangle$, $\langle a^\dagger a \rangle$, $\langle \sigma_k^z \sigma_j^z \rangle$, $\langle \sigma_k^- \sigma_j^- \rangle$. Note that equivalently one could have chosen a different set of variables by, for instance, writing down an equation of motion for the quantity $\langle \sigma_k^+ a \rangle$ instead of $\langle \sigma_k^- a^\dagger \rangle$, as these variables are just the complex conjugates of each other. To obtain a closed set of equations, all the third-order expectation values occurring in (B.1) - (B.12) are truncated according to Eq. (2.14). As an example, we present Eq. (B.6) after the truncation:

$$
\frac{d}{dt} \langle \sigma_k^- a^\dagger \rangle = - \left( \kappa + \gamma_h + 2\gamma_p + i \left( \Delta_k - \Delta_c \right) \right) \langle \sigma_k^- a^\dagger \rangle + \eta \langle \sigma_k^- \rangle + i \sum_{\substack{j=1 \\ j \neq k}}^{N} g_j \langle \sigma_j^+ \sigma_k^- \rangle
$$

$$
+ i \frac{g_k}{2} \left( \langle \sigma_k^z \rangle + 1 \right) + i\, g_k \Big( \langle \sigma_k^z a \rangle^* \langle a \rangle + \langle \sigma_k^z a^\dagger \rangle \langle a \rangle^* + \langle a^\dagger a \rangle \langle \sigma_k^z \rangle
$$

$$
- 2 \langle \sigma_k^z \rangle \langle a \rangle^* \langle a \rangle \Big) . \tag{2.34}
$$

Henceforth, this equation is decoupled from higher-order expectation values. The closed set of equations, obtained by this strategy, can again be solved numerically, for instance, using Runge-Kutta methods. The validity of the second-order cumulant expansion is limited by the approximation that all third-order cumulants vanish $\langle ABC \rangle_c = 0$ (for the example given in Equation (2.34), $\langle \sigma_k^z a^\dagger a \rangle_c = 0$).

**Third-Order Cumulant Expansion**   Finally, we defer the point of truncation once more and consider also all third-order cumulants, except of those including three spin operators. Note that the field operators $a$ and $a^\dagger$ play a prominent role in the system since the cavity mode acts as a collective variable mediating excitations among the individual spins of the ensemble. We therefore treat the third-order cumulants involving field operators preferentially and neglect those involving only spin operators. The set of dynamical variables above is thus extended by 13 additional expectation values: $\langle \sigma_k^z a^\dagger a \rangle$, $\langle \sigma_k^- a^\dagger a \rangle$, $\langle \sigma_k^- a^\dagger a^\dagger \rangle$, $\langle \sigma_k^z aa \rangle$, $\langle \sigma_k^- aa \rangle$, $\langle a^\dagger aa \rangle$, $\langle aaa \rangle$, $\langle \sigma_k^z \sigma_j^z a \rangle$, $\langle \sigma_k^- \sigma_j^- a^\dagger \rangle$, $\langle \sigma_k^+ \sigma_j^- a \rangle$, $\langle \sigma_k^z \sigma_j^- a^\dagger \rangle$, $\langle \sigma_k^z \sigma_j^- a \rangle$, $\langle \sigma_k^- \sigma_j^- a \rangle$. Their temporal evolution is determined by the equations (B.1) - (B.25) given in Appendix B. In order to close this set of equations we use (2.14) and (2.15) for the third-order expectation values including three spin operators and all fourth-order expectation values, respectively.

We demonstrate this procedure on the example of Eq. (B.21):

$$
\frac{d}{dt} \left\langle \sigma_k^- \sigma_j^- a^\dagger \right\rangle \underset{j \neq k}{=} - \left( \kappa + 2\gamma_h + 4\gamma_p + i(\Delta_k + \Delta_j - \Delta_c) \right) \left\langle \sigma_k^- \sigma_j^- a^\dagger \right\rangle + \eta \left\langle \sigma_k^- \sigma_j^- \right\rangle
$$

$$
+ i \sum_{\substack{m=1 \\ m \neq k,j}}^{N} g_m \left\langle \sigma_m^+ \sigma_k^- \sigma_j^- \right\rangle + i\frac{g_k}{2} (\left\langle \sigma_j^- \right\rangle + \left\langle \sigma_k^z \sigma_j^- \right\rangle) + i\frac{g_j}{2} (\left\langle \sigma_k^- \right\rangle + \left\langle \sigma_j^z \sigma_k^- \right\rangle)
$$

$$
+ i\, g_k \left\langle \sigma_k^z \sigma_j^- a^\dagger a \right\rangle + i\, g_j \left\langle \sigma_j^z \sigma_k^- a^\dagger a \right\rangle
$$

The expectation value $\left\langle \sigma_m^+ \sigma_k^- \sigma_j^- \right\rangle$ is expanded according to

$$
\left\langle \sigma_m^+ \sigma_k^- \sigma_j^- \right\rangle = \left\langle \sigma_m^+ \sigma_k^- \right\rangle \left\langle \sigma_j^- \right\rangle + \left\langle \sigma_m^+ \sigma_j^- \right\rangle \left\langle \sigma_k^- \right\rangle + \left\langle \sigma_k^- \sigma_j^- \right\rangle \left\langle \sigma_m^- \right\rangle^*
$$
$$
- 2 \left\langle \sigma_m^- \right\rangle^* \left\langle \sigma_k^- \right\rangle \left\langle \sigma_j^- \right\rangle . \tag{2.35}
$$

Here $m \neq k \neq j$, as otherwise the commutation relations (2.23) enable a reduction of the order of the expectation without any truncation needed. The fourth-order expectation values, $\left\langle \sigma_k^z \sigma_j^- a^\dagger a \right\rangle$ and $\left\langle \sigma_j^z \sigma_k^- a^\dagger a \right\rangle$, respectively, are both treated in the same way,

$$
\left\langle \sigma_k^z \sigma_j^- a^\dagger a \right\rangle = \left\langle \sigma_k^z \right\rangle \left\langle \sigma_j^- a^\dagger a \right\rangle + \left\langle \sigma_j^- \right\rangle \left\langle \sigma_k^z a^\dagger a \right\rangle + \left\langle a \right\rangle^* \left\langle \sigma_k^z \sigma_j^- a \right\rangle + \left\langle a \right\rangle \left\langle \sigma_k^z \sigma_j^- a^\dagger \right\rangle \tag{2.36}
$$

$$
+ \left\langle \sigma_k^z \sigma_j^- \right\rangle \left\langle a^\dagger a \right\rangle + \left\langle \sigma_k^z a^\dagger \right\rangle \left\langle \sigma_j^- a \right\rangle + \left\langle \sigma_k^z a \right\rangle \left\langle \sigma_j^- a^\dagger \right\rangle
$$

$$
- 2 \Big( \left\langle \sigma_k^z \sigma_j^- \right\rangle \left\langle a \right\rangle^* \left\langle a \right\rangle + \left\langle \sigma_k^z a^\dagger \right\rangle \left\langle \sigma_j^- \right\rangle \left\langle a \right\rangle + \left\langle \sigma_k^z a \right\rangle \left\langle \sigma_j^- \right\rangle \left\langle a \right\rangle^*
$$

$$
+ \left\langle \sigma_j^- a^\dagger \right\rangle \left\langle \sigma_k^z \right\rangle \left\langle a \right\rangle + \left\langle \sigma_j^- a \right\rangle \left\langle \sigma_k^z \right\rangle \left\langle a \right\rangle^* + \left\langle a^\dagger a \right\rangle \left\langle \sigma_k^z \right\rangle \left\langle \sigma_j^- \right\rangle \Big)
$$

$$
+ 6 \left\langle \sigma_k^z \right\rangle \left\langle \sigma_j^- \right\rangle \left\langle a \right\rangle^* \left\langle a \right\rangle ,
$$

where again $k \neq j$. Equation (B.21) is then decoupled from all higher-order expectation values. Applying this procedure to all equations of motion for operators of third-order (B.13) - (B.25) results in a closed set of equations.

Once this is accomplished - no matter through which truncation scheme - the closed set of equations can be solved numerically. We reveal the system's dynamics by a straight forward Runge-Kutta integration [54] for well defined initial conditions. Furthermore, we are interested in the stationary solutions or steady-states, which demonstrate various nonlinear effects such as bistability within a certain interval of the driving signal $\eta$. The steady-state solutions are found by setting all time derivatives to zero and by solving the obtained algebraic set of equations by a modification of the Powell hybrid method [55]. The results for both, stationary states and dynamics of the system, are shown in Chapter 3 for distinct physical systems. In each case we compare the results obtained from the different truncation methods, ranging from the simple linear model to the intricate third-order cumulant expansion developed in this section.

## 2.3. Clustering of Large Spin Ensembles

The main goal of this thesis is the development of a rigorous model for large and inhomogeneously broadened spin ensembles coupled to a single cavity mode in the presence of strong external driving. Up to now we showed how cumulant expansion methods of increasing orders can be implemented to account for rising correlations due to increasing driving powers; however, we did not care about the system size. The first-order cumulant expansion method is based on the equations (2.29) - (2.31), which can be written as $3N + 2$ real-valued equations (2 and $2N$ for the complex valued quantities $\langle a \rangle$ and $\langle \sigma_k^- \rangle$, as well as $N$ for the real valued expectation values $\langle \sigma_k^z \rangle$). For the second- and third-order cumulant expansion the amount of real-valued equations is given by $4N^2 + N(N-1)/2 + 5N + 5$ and $13N^2 + N(N-1)/2 + 5N + 9$, respectively. Hence, even for the highest order of the cumulant expansion methods regarded in this thesis, the computational effort grows only quadratically with the number of spins in the ensemble[8], which is indeed remarkable considering the exponential growth of the corresponding Hilbert space. Nevertheless, a further reduction of the configuration space is indispensable, since we aim to describe very large ensembles of up to about $10^{15}$ spins ($N \approx 10^{12}$ for a typical nitrogen-vacancy setup, as used in [31–33]).

The use of collective spin operators, $\hat{J}_z = \sum_k \sigma_k^z$, is a well-established approach in many-particle quantum optics. However, the inhomogeneous broadening of the spin ensemble complicates matters to some degree. For the present thesis we decided to adopt this procedure in a fairly simple way. Since deriving the equations of motion (B.1) - (B.25) for the individual spins (no matter how many spins there actually are) is not the difficult part (rather than solving them), we cluster the equations themselves. As long as the distributions of the expectation values describe smooth functions in frequency, it is perfectly valid to group them in small frequency clusters and solve only one equation per cluster; this procedure, illustrated in Figure (2.3), corresponds to a plain discretization (or better "re-discretization") method.

We demonstrate this clustering for the coupled equations (B.1), (B.2), and (B.4). For simplicity we consider only the inhomogeneous frequency distribution of the spin ensemble and omit any inhomogeneities of the coupling strengths. In general the $g_k$ can possess a frequency as well as a spatial dependence; however we assume that the coupling is homogeneous within the whole cavity and set $g_k = g$. Starting from the equation for the collective quantity $\langle a \rangle$, we rearrange the sum, $\sum_{k=1}^N$, to

---

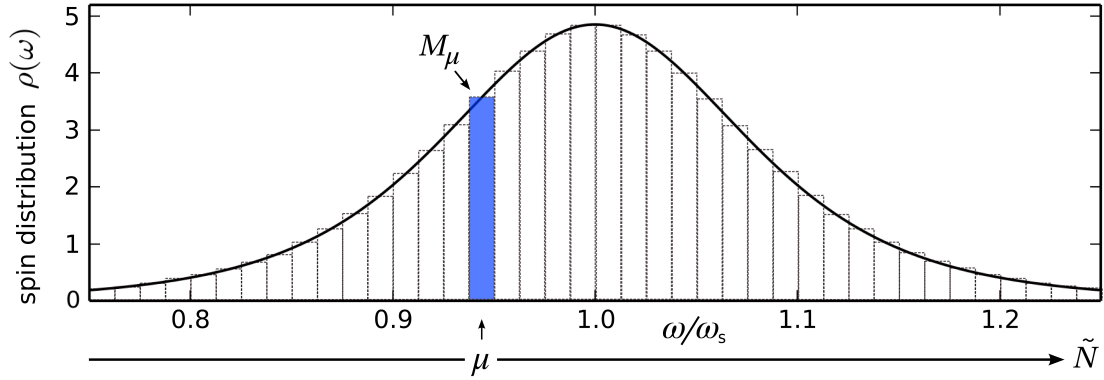[8] ...since we neglect cumulants involving three spin operators.

Figure 2.3.: Clustering of an inhomogeneous spin distribution. The continuous spin distribution $\rho(\omega)$ is grouped into $\tilde{N}$ equidistant frequency clusters (*dashed bars*), which are labeled by Greek indices. Within each cluster we assume a constant detuning from the central frequency $\omega_s$. Consequently, the equations of motion have to be solved only once per cluster, since for instance $\langle \sigma^-_{k_\mu} \rangle = \langle \sigma^-_{j_\mu} \rangle$. The $\mu$-th cluster that contains $M_\mu$ spins is highlighted in *blue*. A sum over all spins inside this cluster, $\sum_{k_\mu=1}^{M_\mu} \langle \sigma^-_{k_\mu} \rangle$, is replaced by the multiplication $M_\mu \langle \sigma^-_{k_\mu} \rangle$.

$\tilde{N}$ equidistant frequency clusters;

$$\frac{d}{dt} \langle a \rangle = -(\kappa + i\,\Delta_c)\,\langle a \rangle - ig \sum_{k=1}^{N} \langle \sigma^-_k \rangle + \eta$$

$$= -(\kappa + i\,\Delta_c)\,\langle a \rangle - ig\Big( \underbrace{\sum_{k_1=1}^{M_1} \langle \sigma^-_{k_1} \rangle}_{M_1 \langle \sigma^-_{k_1} \rangle} + \ldots + \underbrace{\sum_{k_\mu=1}^{M_\mu} \langle \sigma^-_{k_\mu} \rangle}_{M_\mu \langle \sigma^-_{k_\mu} \rangle} + \ldots + \underbrace{\sum_{k_{\tilde{N}}=1}^{M_{\tilde{N}}} \langle \sigma^-_{k_{\tilde{N}}} \rangle}_{M_{\tilde{N}} \langle \sigma^-_{k_{\tilde{N}}} \rangle} \Big) + \eta\,,$$

where the Greek indices, running from 1 to $\tilde{N}$, label the different frequency clusters. Hence, $\langle \sigma^-_{k_\mu} \rangle$ is the expectation value corresponding to the $k$-th spin in the $\mu$-th cluster and $M_\mu$ gives the number of spins within that cluster. Clearly, all $M_\mu$ sum up to the total number of spins, $\sum_{\mu=1}^{\tilde{N}} M_\mu = N$. As indicated above we assume in the following that the expectation values are constant within each cluster;

$$\frac{d}{dt} \langle a \rangle = -(\kappa + i\,\Delta_c)\,\langle a \rangle - ig\Big( M_1 \langle \sigma^-_{k_1} \rangle + \ldots + M_\mu \langle \sigma^-_{k_\mu} \rangle + \ldots + M_{\tilde{N}} \langle \sigma^-_{k_{\tilde{N}}} \rangle \Big) + \eta$$

$$= -(\kappa + i\,\Delta_c)\,\langle a \rangle - ig \sum_{\mu=1}^{\tilde{N}} M_\mu \langle \sigma^-_{k_\mu} \rangle + \eta\,.$$

Note that here the sum stretches from 1 to $\tilde{N}$. Consequently, the equation for $\langle \sigma^-_k \rangle$

has to be solved only once for each cluster $\mu$;

$$\frac{d}{dt}\langle\sigma_{k_\mu}^-\rangle = -(\gamma_h + 2\gamma_p + i\,\Delta_{k_\mu})\,\langle\sigma_{k_\mu}^-\rangle + i\,g\,\langle\sigma_{k_\mu}^z a\rangle\ .$$

The same clustering also applies to equations for expectation values of higher order:

$$\frac{d}{dt}\langle\sigma_{k_\mu}^z a\rangle = -(\kappa + 2\gamma_h + i\,\Delta_c)\,\langle\sigma_{k_\mu}^z a\rangle - 2\gamma_h\,\langle a\rangle + \eta\,\langle\sigma_{k_\mu}^z\rangle$$

$$- ig\Big(\underbrace{\sum_{j_1=1}^{M_1}\langle\sigma_{k_\mu}^z\sigma_{j_1}^-\rangle}_{M_1\langle\sigma_{k_\mu}^z\sigma_{j_1}^-\rangle} + \ldots + \underbrace{\sum_{\substack{j_\mu=1\\j_\mu\neq k_\mu}}^{M_\mu}\langle\sigma_{k_\mu}^z\sigma_{j_\mu}^-\rangle}_{(M_\mu-1)\langle\sigma_{k_\mu}^z\sigma_{j_\mu}^-\rangle} + \ldots + \underbrace{\sum_{j_{\tilde N}=1}^{M_{\tilde N}}\langle\sigma_{k_\mu}^z\sigma_{j_{\tilde N}}^-\rangle}_{M_{\tilde N}\langle\sigma_{k_\mu}^z\sigma_{j_{\tilde N}}^-\rangle}\Big)$$

$$+ ig\,\langle\sigma_{k_\mu}^-\rangle + 2i\,g(\langle\sigma_{k_\mu}^- a^\dagger a\rangle - \langle\sigma_{k_\mu}^- a^\dagger a^\dagger\rangle^*)$$

$$= -(\kappa + 2\gamma_h + i\,\Delta_c)\,\langle\sigma_{k_\mu}^z a\rangle - 2\gamma_h\,\langle a\rangle + \eta\,\langle\sigma_{k_\mu}^z\rangle - ig\sum_{\nu=1}^{\tilde N}M_\nu\,\langle\sigma_{k_\mu}^z\sigma_{j_\nu}^-\rangle$$

$$+ ig\,\langle\sigma_{k_\mu}^z\sigma_{j_\mu}^-\rangle + ig\,\langle\sigma_{k_\mu}^-\rangle + 2i\,g(\langle\sigma_{k_\mu}^- a^\dagger a\rangle - \langle\sigma_{k_\mu}^- a^\dagger a^\dagger\rangle^*)$$

All other equations (B.1) - (B.25) are treated accordingly.

The amount of required equations thus depends on the number of clusters $\tilde N$, which is a tremendous reduction as compared to the total number of spins $N$. The actual number of equations that have to be solved for the different orders of cluster expansions are summarised in Table 2.1.

Table 2.1.

| Cumulant Expansion (CE) | Number of Equations |
|---|---:|
| 1st-order CE | $3\tilde N + 2$ |
| 2nd-order CE | $4\tilde N^2 + \tilde N(\tilde N + 1)/2 + 11\tilde N + 5$ |
| 3rd-order CE | $13\tilde N^2 + \tilde N(\tilde N + 1)/2 + 23\tilde N + 9$ |

Note that some expectation values, like $\langle\sigma_{k_\mu}^z\sigma_{j_\nu}^z\rangle$, are symmetric in the indices $\mu$ and $\nu$, a fact which has to be appropriately taken into consideration for the number of equations. Hence the quantity $\langle\sigma_{k_\mu}^z\sigma_{j_\nu}^z\rangle$, for instance, demands only $\tilde N(\tilde N + 1)/2$ equations, rather than $\tilde N^2$. An important technical difference between the clustered and "unclustered" case arise for the diagonal elements of expectation

values including two spin operators. In contrast to the case without clusters, where the diagonal elements $k = j$ of such expectation values drop out, in the clustered case the diagonal elements $\mu = \nu$ have to be considered, since they account for different spins but within the same cluster.

# Chapter 3.

# Results and Discussion

In this chapter we apply the cumulant expansion (CE) approach developed above on the Tavis-Cummings model for three very different physical situations of increasing complexity. We start with a single spin inside the cavity ($N = 1$), which corresponds to the well studied Jaynes-Cummings model. Following that, the number of spins is increased ($N = 3$) to make for a basic test on spin-spin correlations. These first two realizations provide an ideal test on the validity of our approach, since the moderate system sizes enable an exact numerical solution of the problem via direct integration of the master equation [56][9], which serves us as a benchmark for the developed CE approach. Finally, we apply our model to a real physical system involving a large inhomogeneously broadened spin ensemble. The parameters we used throughout our calculations are summarized in the table below and correspond to the values in the experimental realization [31], which we aim to describe in Section 3.3.

Table 3.1.

| Parameters | | | |
|---|---|---|---|
| cavity frequency | . . . | $\omega_c/2\pi\ =$ | 2.6915 GHz |
| cavity losses | . . . | $\kappa\ /2\pi\ =$ | 0.4 MHz |
| spin losses (non-radiative) | . . . | $\gamma_p/2\pi\ =$ | 20 kHz |
| spin losses (radiative) | . . . | $\gamma_h/2\pi\ =$ | 1 kHz |

In our calculations we assume that the driving field as well as the central spin of the ensemble is on resonance with the cavity frequency $\omega_c = \omega_p = \omega_s$.

---

[9] Note that such direct integration methods are always severely limited in the size of the considered system. For the software package [57, 58] that we use in our calculations, the maximal number of spins that can be handled in an open quantum system is approximately $N = 12$.

# 3.1. The Jaynes-Cummings Model

In Section 2.2 we developed the CE approach for the Tavis-Cummings model, which can be considered as the many-spins generalization of the well known Jaynes-Cummings model. Setting $N = 1$ in Eq. (2.21) gives the Jaynes-Cummings Hamiltonian,

$$H = \omega_c a^\dagger a + \frac{1}{2}\omega_s \sigma^z + g\left(\sigma^- a^\dagger + \sigma^+ a\right) + i\left(\eta\, a^\dagger e^{-i\omega_p t} - \eta^* a\, e^{i\omega_p t}\right), \qquad (3.1)$$

where we omit the index $k = 1$ for the spin operators and write $\omega_s$ for the frequency of the single spin. The Lindblad term (2.22) is simplified accordingly,

$$\begin{aligned} \mathcal{L}(\rho) &= \kappa\left(2a\rho a^\dagger - a^\dagger a\,\rho - \rho\, a^\dagger a\right) + \gamma_h\left(2\sigma^-\rho\,\sigma^+ - \sigma^+\sigma^-\rho - \rho\,\sigma^+\sigma^-\right) \\ &\quad + \gamma_p\left(\sigma^z\rho\,\sigma^z - \rho\right). \end{aligned} \qquad (3.2)$$

Indeed the corresponding master equation for the Jaynes-Cummings model can be solved directly by numerical integration [57, 58], which serves as a benchmark for the approximation schemes developed in this thesis. We will refer to the solution obtained by the direct methods as the exact solution, since they account for the full quantum mechanical problem taking into account exactly all correlations within the system. In the following we calculate both, the stationary states and the dynamical evolution of the system using the Holstein-Primakoff approximation and the CE method. The resulting solutions will then be compared with the exact ones. Clearly, since $N = 1$, all equations of motion for expectation values involving more than one spin operator drop out and we end up with a reduced set of equations, which serves as an optimal starting point to apply our truncation procedure.

**Stationary States**   While the cavity is driven with a constant external field $\eta(t) = \eta$, the system settles after some time into a stationary state due to the dissipative processes characterized by $\kappa$, $\gamma_h$, and $\gamma_p$. These stationary states typically give rise to nonlinear behaviour with respect to the driving field amplitude $\eta$, such as optical bistability [15], and thereby provide an interesting test for our model. The stationary solutions are calculated by setting all time-derivatives in the corresponding equations (B.1) - (B.25) to zero and by solving the resulting algebraic equations numerically. For this purpose we use a modification of the Powell hybrid method [55]. Figure 3.1 shows the stationary states obtained by the CE of first-, second-, and third-order as well as the exact solution obtained from the master equation. The results are presented for three different coupling strengths $g/2\pi = 0.5\,\text{MHz}$, $2\,\text{MHz}$, and $8\,\text{MHz}$. The stationary transmission through the cavity, being proportional to the cavity probability amplitude $|\langle a_{st}\rangle|^2$ (shown in the left column of Figure 3.1), typically consists of two branches, the low- and the high-transmission branch, which merge into each other via some nonlinear region
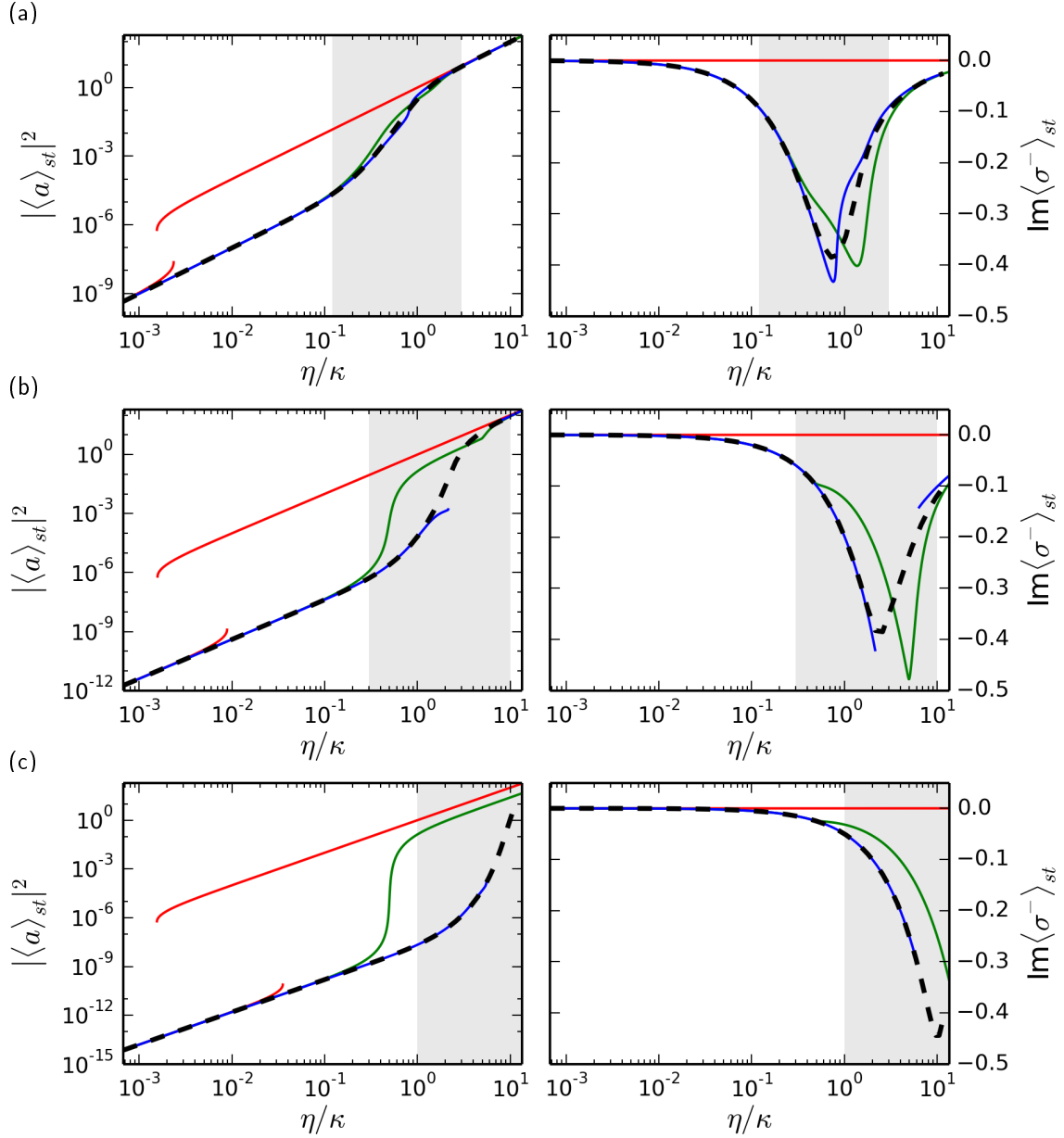
(a)

(b)

(c)



Figure 3.1.: Stationary states versus the normalized driving amplitude $\eta/\kappa$ ($\kappa/2\pi = 0.4$ MHz) for $N = 1$ and increasing coupling strengths $g/2\pi$ (a)-(c). *Left column:* Steady-state solution of the cavity probability amplitude $|\langle a \rangle_{st}|^2$. *Right column:* Steady-state $\langle \sigma^- \rangle_{st}$ of the spin operator $\sigma^-$, whose expectation value is purely imaginary in the absence of detuning, $\Delta_s = 0$. The solutions obtained from the 1st-, 2nd-, and 3rd-order CE are shown by the *red, green,* and *blue solid lines,* whereas the exact solution is represented by the *dashed black line.* The *grey area* indicates the nonlinear regime for which the cavity probability amplitude does not scale with the driving power ($|\langle a \rangle_{st}|^2 \not\propto |\eta|^2$). The results are shown for three different coupling strengths $g/2\pi$: (a) $0.5$ MHz, (b) $2$ MHz, and (c) $8$ MHz.

(grey area in Figure 3.1). Below and above that region the system behaves linearly, which means that the expectation values such as $\langle a(t) \rangle$ scale linearly with the driving field amplitude $\eta$ ($\langle a(t) \rangle \propto \eta$). Such a behaviour is indicated by the linear growth of the steady-state transmission in log-log scale as shown in the left column of Figure 3.1. The levels of the transmission branches are well described by the first-order CE only in the limits $\eta \to 0$ and $\eta \gg 1$. The first-order CE, however, overestimates the nonlinearity, since it predicts a bistable behaviour for the cavity probability amplitude $|\langle a \rangle_{st}|^2$. Figure 3.1 shows that the actual nonlinear behaviour of the system starts at higher driving field amplitudes than predicted by the first-order CE and is also much less pronounced. Furthermore, also the dip in the stationary state of $\langle \sigma^- \rangle$, which occurs in the nonlinear regime, can not be resolved, as shown in the right column of Figure 3.1. In order to describe the nonlinearity of the steady-states correctly, higher-order correlations within the system have to be considered. The presented figure shows that the results obtained from the second- and third-order CE agree reasonably well with the exact solution for $g/2\pi = 0.5\,\text{MHz}$. Increasing the coupling strength, however, also increases the correlations within the system. As a consequence, for $g/2\pi > 0.5\,\text{MHz}$ the results from the second-order CE start to deviate significantly from the exact solution for $\eta/\kappa > 0.5$. If we turn to the third-order CE, no stable solutions can be found in the strong nonlinear regime, that is for $\eta/\kappa > 1.5$ and $6$, respectively, but below these critical values the third-order CE gives a perfect agreement with the exact solutions.

It is therefore shown that the CE approach provides a promising method to investigate the nonlinear steady-state regime where correlations of the system can play an important role.

**Dynamics**   Following the investigation of stationary solutions, we are also interested in the dynamical evolution of the system under a constant driving field. Initially, at $t = t_0 = 0$, the system is in its ground state, with the cavity being empty, $\langle a(t_0) \rangle = 0$, and the spin resting at the lowest point of the Bloch-sphere, $\langle \sigma^z(t_0) \rangle = -1$ and $\langle \sigma^-(t_0) \rangle = 0$. When the constant driving field is switched on, the cavity field amplitude starts to oscillate, since the system is in the strong-coupling regime where the spin-coupling exceeds the total losses ($g > \kappa + \gamma_h + \gamma_p$) and thereby allows for a Non-Markovian feedback [15]. After some of these Rabi-oscillations the system finally settle to a stationary value (depicted in Figure 3.1). In the following we calculate the dynamical evolution of the system via Runge-Kutta integration of the corresponding equations of motion using the Holstein-Primakoff approximation as well as the CE methods and compare our results with the exact solution. The initial conditions for higher-order expectation values can be derived from the first-order expectation values, since at $t = 0$ the system is uncorrelated, which allows for a full factorization of all expectation values ($\langle \sigma^z a(t_0) \rangle = \langle \sigma^z(t_0) \rangle \langle a(t_0) \rangle$).

Figures 3.2 and 3.3 provide the temporal evolution of the cavity probability am-
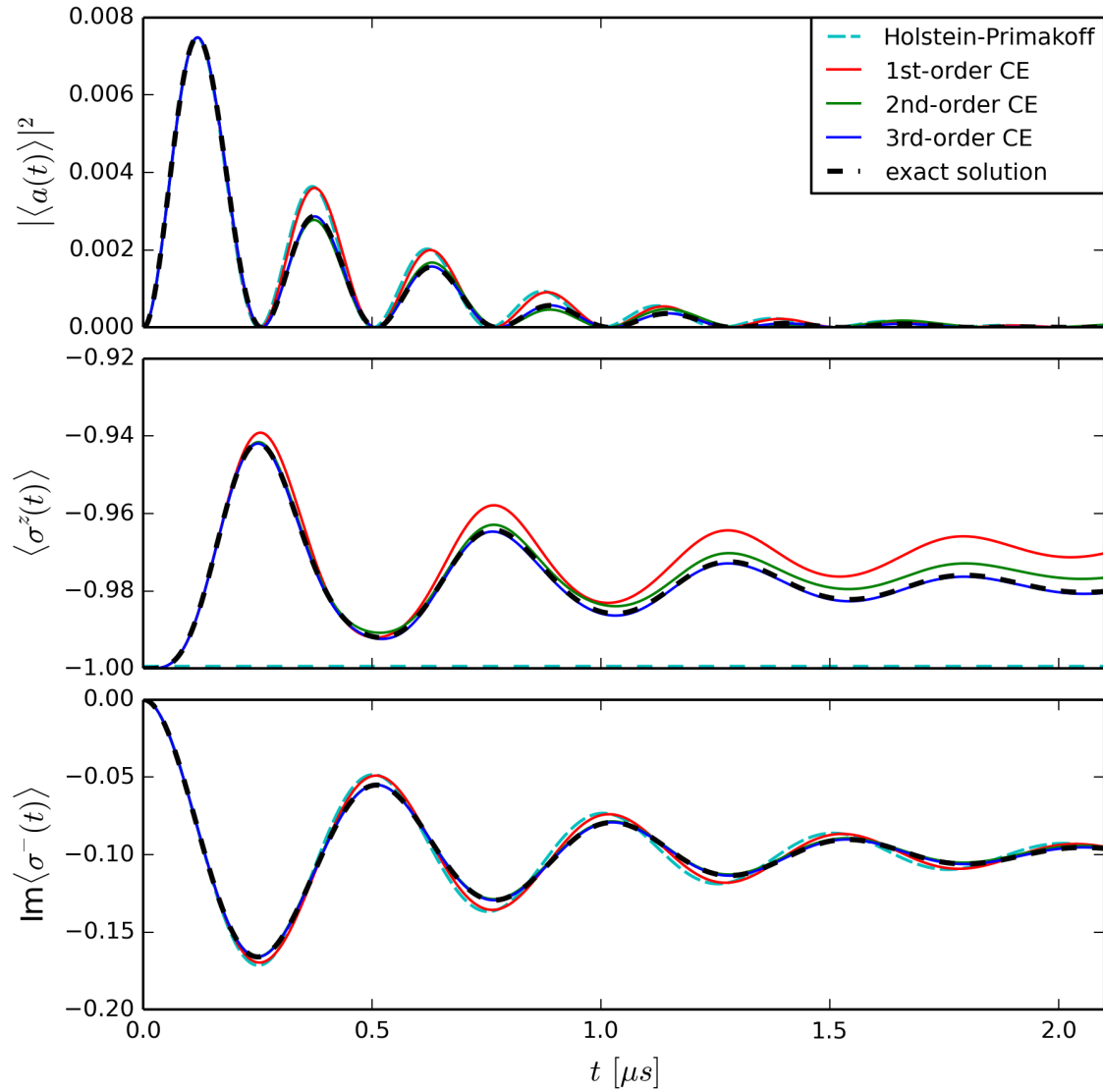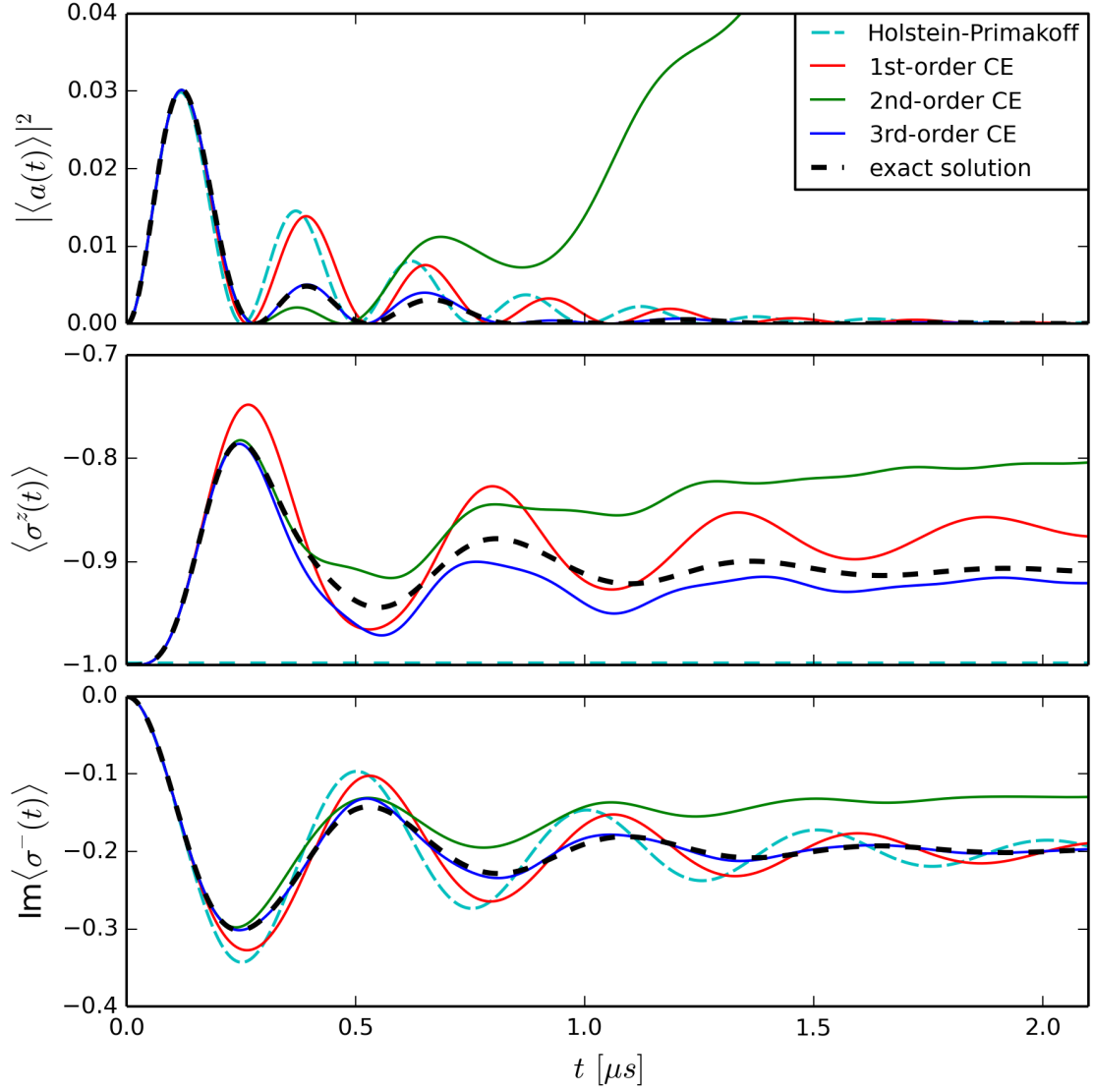
Figure 3.2.: Dynamics of the cavity probability amplitude $|\langle a(t) \rangle|^2$ as well as the spin operators $\langle \sigma^z \rangle$ and $\langle \sigma^- \rangle$ for the coupling strength $g/2\pi = 2\,\text{MHz}$. A constant driving field of amplitude $\eta/\kappa = 0.5$ ($\kappa/2\pi = 0.4$ MHz) is applied for $t \geq 0$. Results from the Holstein-Primakoff approximation are shown by the *dashed cyan line*; solutions obtained by 1st-, 2nd-, and 3rd-order CE are shown by *solid lines* in *red, green,* and *blue*, respectively, and the exact solution is represented by the *dashed black line*.

Figure 3.3.: Dynamics of the cavity probability amplitude $|\langle a(t)\rangle|^2$ as well as the spin operators $\langle \sigma^z \rangle$ and $\langle \sigma^- \rangle$ for the coupling strength $g/2\pi = 2\,\mathrm{MHz}$. A constant driving field of amplitude $\eta/\kappa = 1$ ($\kappa/2\pi = 0.4$ MHz) is applied for $t \geq 0$. Results from the Holstein-Primakoff approximation are shown by the *dashed cyan line*; solutions obtained from the 1st-, 2nd-, and 3rd-order CE are shown by *solid lines* in *red, green, and blue*, respectively, and the exact solution is represented by the *dashed black line*.

plitude $|\langle a(t) \rangle|^2$ as well as the spin operators $\langle \sigma^z(t) \rangle$ and $\mathrm{Im} \langle \sigma^-(t) \rangle$ for a coupling strength of $g/2\pi = 2\,\mathrm{MHz}$ and driving field amplitudes of $\eta/\kappa = 0.5$ and $1.0$, respectively. In the first case the system just started to enter the nonlinear regime, as the spin excitations $\langle \sigma^z(t) \rangle$ are still rather weak (no more than 5% from the initial alignment $\langle \sigma^z \rangle = -1$ during the first Rabi-cycle). Nevertheless, this small deviation from the south-pole of the Bloch-sphere already alters the evolution of the cavity amplitude significantly with respect to the Holstein-Primakoff approximation ($\langle \sigma^z(t) = -1 \rangle$), as shown in the upper panel of Figure 3.2. The relative error $\delta \left| \langle a(t) \rangle \right|^2_{H.P.} = \left( \left| \langle a(t) \rangle \right|^2_{H.P.} - \left| \langle a(t) \rangle \right|^2_{exact} \right) / \left| \langle a(t) \rangle \right|^2_{exact}$ for the cavity probability amplitude obtained from the Holstein-Primakoff approximation equals $0.27$ at the position of the second Rabi-peak ($t = 3.8\,\mu s$). Interestingly, although the first-order CE captures the evolution of the spin fairly well for the first 0.6 microseconds, the improvement in the evolution of the cavity field amplitude with respect to the Holstein-Primakoff approximation is rather weak. In order to describe the systems's dynamics correctly, the correlations between the cavity field and the single spin have to be considered. Indeed, for the parameters used in Figure 3.2 the second-order CE significantly improves the obtained results and third-order CE already gives a perfect agreement with the exact solution.

When the driving field amplitude is increased to $\eta/\kappa = 1.0$, the deviations in the results obtained from the different methods become more apparent (see Figure 3.3). The Holstein-Primakoff approximation gives the same behaviour of the system as already shown in Figure 3.2, but multiplied by a factor of 4, since this model is linear in $\eta$. Although the Holstein-Primakoff approximation still works fine for short times and accounts correctly for the first Rabi-peak of the cavity probability amplitude, the subsequent peaks of the exact solution are clearly suppressed as compared to the linear model, due to the formation of correlations within the system. As was already shown in the steady-state analysis, the second-order CE tends towards another stationary state characterized by a large steady-state transmission and represented by the green curves in Figure 3.1 (which is in agreement with our dynamical studies). Note that also the first-order CE gives the wrong stationary state, as calculated above, but it settles at this value at a much later time, which is not shown in the figure. Albeit the first- and second-order CE fail to describe the dynamics correctly for the present driving field amplitude, Figure 3.3 shows that the third-order CE reproduces the exact solutions rather well.

In summary these first results provide important insights into the applicability of our model. First of all, the third-order CE is sufficient to accurately describe the dynamics as well as the stationary solutions of the system under consideration for a broad range of coupling strengths and driving fields notably beyond the linear regime. The third-order CE fails though for high coupling strengths and strong driving fields, where cumulants of higher order gain significance (results not shown). However, the presented results indicate that our strategy, to employ higher

and higher orders of cumulants in order to account for the correlations within the system, works fine.

## 3.2. Three Spins Coupled to the Cavity

Before we move on to the challenging case of inhomogeneous broadening and very large spin ensembles, we test the CE technique on the Tavis-Cummings model including three spins inside the cavity. We follow the same procedure as for the single spin case, but now with two additional spins at frequencies $\omega_{1,3} = \omega_2 \mp \Delta\omega$, where $\omega_2$ is the frequency of the central spin, which is on resonance with the cavity and the driving field ($\omega_2 = \omega_c = \omega_p = 2.6915\,\mathrm{GHz}$), and $\Delta\omega = 50\,\mathrm{kHz}$. For reasons of comparison we introduce the collective coupling strength $\Omega := \sqrt{N}g$. Thus, in order to achieve the same collective coupling as in the single-spin case, the individual coupling strength $g$ of the $N = 3$ spins is reduced by a factor $1/\sqrt{3}$. We proceed in our calculations as in the previous section of a single spin, however, here the set of equations (B.1) - (B.25) include also expectation values which contain pairs of spin operators.

**Stationary States**  Figure 3.4 compares the results obtained from the first-, second-, and third-order CE with the exact solution for two different collective coupling strengths $\Omega/2\pi = 0.1\,\mathrm{MHz}$ and $0.5\,\mathrm{MHz}$. In the first case the nonlinearity is rather small. In fact there is only a slight change in the slope of the cavity probability amplitude $|\langle a(\eta)\rangle_{st}|^2$ as shown in Figure 3.4 (a), however the first-order CE clearly deviates from the exact solution for driving fields between $\eta/\kappa = 10^{-3}$ and 1, which indicates that the correlations within the system already play an important role. The second- and third-order CE both perfectly agree with the exact solution. For $\Omega/2\pi = 0.5\,\mathrm{MHz}$, however, the second-order CE starts to deviate from the exact solution at driving fields $\eta/\kappa > 0.2$ and also the third-order CE fails to account for the nonlinear regime correctly. In particular the dip in the stationary value of $\mathrm{Im}\,\langle\sigma_2^-\rangle$, shown in the right column of Figure 3.4(b), can not be resolved.

**Dynamics**  If we now turn to the dynamical evolution of the system we restrict our investigation to the case $\Omega/2\pi = 0.1\,\mathrm{MHz}$, where the stationary states can be described by the CE pretty well. Figure 3.5 shows the dynamics of the cavity probability amplitude $|\langle a(t)\rangle|^2$ and the spin operators $\langle\sigma_{2,3}^z(t)\rangle$ as well as $\langle\sigma_{2,3}^-(t)\rangle$ for $\eta/\kappa = 0.5$. Since the expectation values $\langle\sigma_{1,2,3}^z(t)\rangle$ take values significantly beyond the south-pole of the Bloch-sphere, it is apparent that the Holstein-Primakoff approximation can not describe the dynamics of the system correctly. After a few microseconds the exact solution for $|\langle a(t)\rangle|^2$ settles at values considerably beyond those predicted by the linear theory. Comparing the results obtained from the first-order CE with the exact solutions suggests that correlations form inside the system within a few microseconds only; for $t < 8\,\mu s$ the first-order CE reproduces the exact solution for the collective quantity $|\langle a(t)\rangle|^2$ quite well, however, for larger times the first-order CE is insufficient to account for the dynamics correctly and cumulants
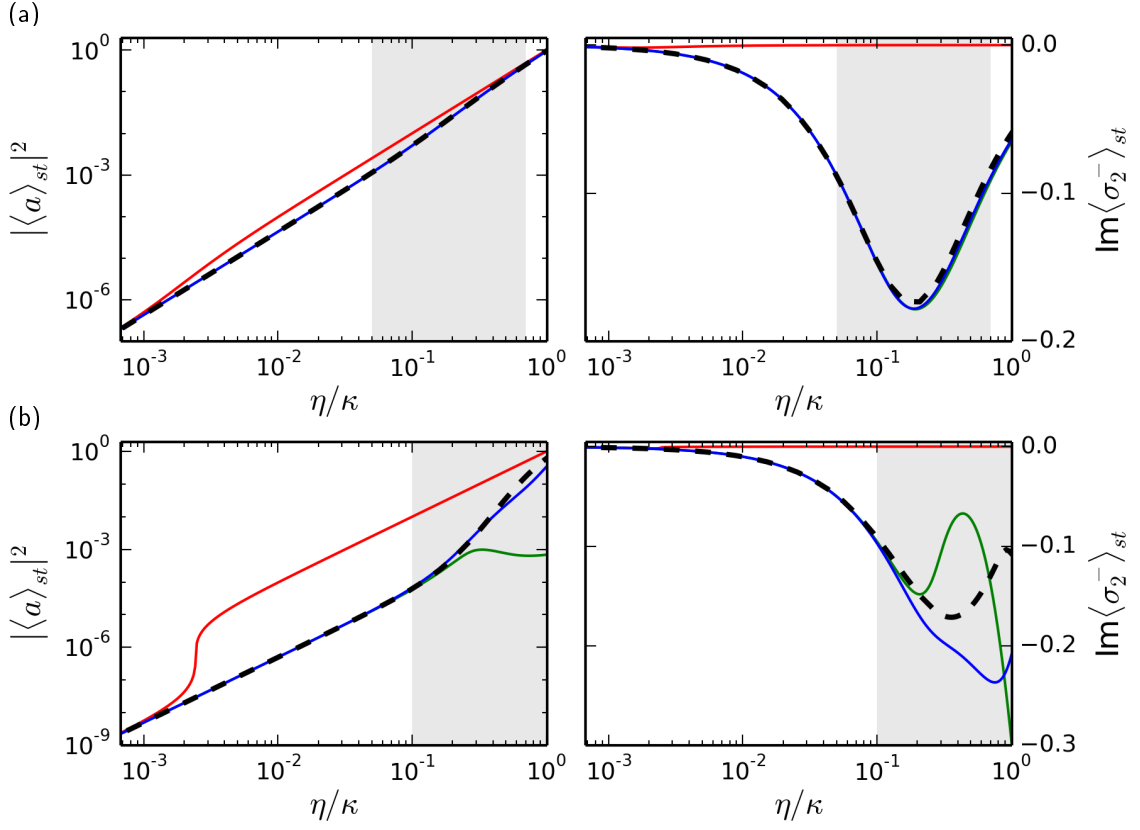
Figure 3.4.: Stationary states versus the normalized driving amplitude $\eta/\kappa$ ($\kappa/2\pi = 0.4$ MHz) for $N = 3$ and two different collective coupling strength $\Omega/2\pi = 0.1$ MHz (a) and $0.5$ MHz (b). *Left panel:* Steady-state solution of the cavity probability amplitude $|\langle a \rangle_{st}|^2$. *Right panel:* Imaginary part of the steady-state $\langle \sigma_2^- \rangle_{st}$ of the central spin operator $\sigma_2^-$, whose expectation value is purely imaginary in the absence of detuning, $\Delta_2 = 0$. The solutions obtained from the 1st-, 2nd-, and 3rd-order CE are represented by the *red, green,* and *blue solid lines,* whereas the exact solution is represented by the *dashed black line.* Note that for (a) the solution of the 2nd- and 3rd-order CE lay on top of each other. The *grey area* indicates the nonlinear regime for which the cavity probability amplitude does not scale with the driving power ($|\langle a \rangle_{st}|^2 \not\propto |\eta|^2$).

of higher order have to be considered. As can be seen from Figure 3.5 already the second-order CE perfectly agree with the exact solution. Here the third-order CE do not provide any new information about the system, which suggests that all third-order cumulants are negligible small.

Overall, these results indicate that the CE approach can be applied on the Tavis-Cummings model, even in the presence of spin-spin correlations. Of course, our approach is always limited by the amount of correlations within the system. For high coupling strengths and large driving fields, many more orders of cumulants have to be considered to keep track of the formation of correlations inside the system. However, the presented results strongly support the hypothesis that the model developed during this thesis is an appropriate and powerful method to investigate interesting quantum optical systems beyond the linear regime.
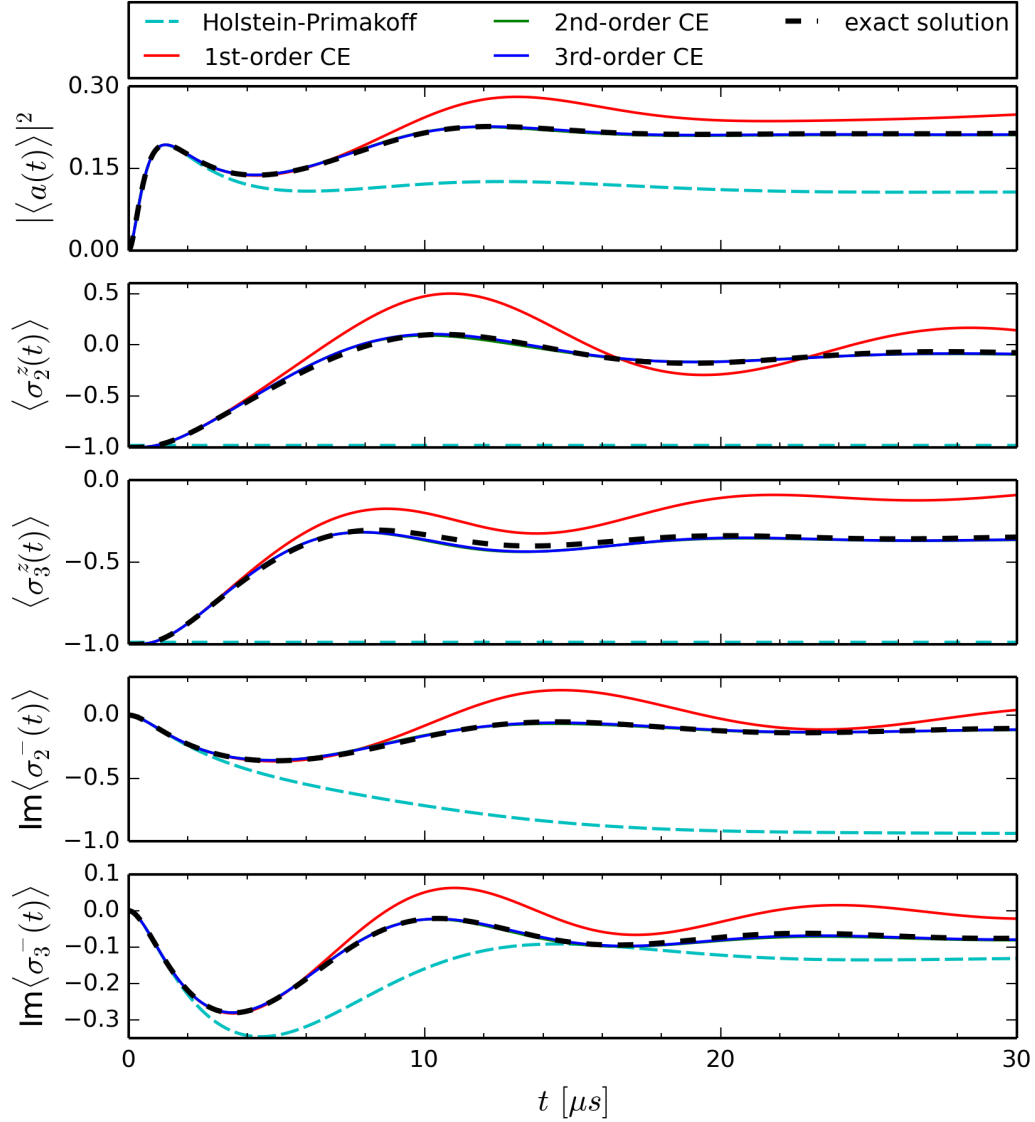
Figure 3.5.: Dynamics of the cavity probability amplitude $|\langle a(t)\rangle|^2$ as well as the spin expectation values $\langle \sigma^z_{2,3}\rangle$ and $\langle \sigma^-_{2,3}\rangle$ for $N = 3$ and the collective coupling strength $\Omega/2\pi = 0.1\,\mathrm{MHz}$. A constant driving field of amplitude $\eta/\kappa = 0.5$ ($\kappa/2\pi = 0.4$ MHz) is applied for $t \geq 0$. Results from the Holstein-Primakoff approximation are shown by the *dashed cyan line*; solutions obtained from the 1st-, 2nd-, and 3rd-order CE are shown by *solid lines* in *red, green,* and *blue,* respectively, and the exact solution is represented by the *dashed black line*. Note that the solution of the 2nd- and 3rd-order CE lie on top of each other.

# 3.3. Inhomogeneous Spin Ensemble

Finally, we apply our model to a very large and inhomogeneously broadened ensemble of spins. In particular we consider a specific experimental realization based on negatively charged nitrogen-vacancy (NV) centers in diamond coupled to a superconducting coplanar waveguide resonator [31]. A brief discussion of the NV center and the experiment, which was carried out at the Atominstitut of the Vienna University of Technology, is given in Appendix C. In previous studies [31–33], the temporal evolution of the system was investigated in the limit of weak driving fields, where the cavity amplitude scales linearly with the driving field. In this section we calculate the dynamics using the CE approach developed in Section 2.2 and compare our results with the experimental data obtained in the nonlinear regime.

The temporal evolution of the system is probed in the following way: Starting from an unexcited ensemble and an empty cavity at $t_0 = 0$ ($\langle \sigma^z_{k_\mu}(t_0) \rangle = \langle \sigma^-_{k_\mu}(t_0) \rangle = 0$ for all spins and $\langle a(t_0) \rangle = 0$), a constant driving field $\eta(t) = \eta$ is applied for about $0.8\,\mu s$. After that the driving field is switched off, $\eta(t > 0.8\,\mu s) = 0$, and the system evolves freely. In our calculations we employ the clustering procedure developed in Section 2.3 and gather the spins in equidistant frequency groups. Typically we use roughly 250 of such clusters. We check explicitly that the physics does not depend on the number of clusters used while making sure that the spin distribution, given by Eq. (C.1), is well resolved and that the revival time $t_r = 2\pi/(\omega_\mu - \omega_{\mu+1})$, introduced through the frequency spacing between adjacent clusters, does not enter in the evolution of the system.

The collective coupling strength achieved in the experiment was $\Omega/2\pi = \sqrt{N}g/2\pi = 8.3\,\text{MHz}$, where the number of spins $N$ inside the ensemble is $\sim 10^{12}$; the other parameters that are used in our calculations can be found in Table 3.1.

**Linear Regime** We start our analysis in the limit of weak driving fields, where the number of spin excitations is negligible as compared to the total number of spins coupled to the cavity. Consequently, the system's dynamical variables scale with the driving field amplitude (for instance $\langle a(t) \rangle \propto \eta$). Of course, here the CE approach should give the same results as the Holstein-Primakoff approximation, which already proved to be a powerful model in this linear regime. Figure 3.6 compares the results of our calculations obtained from the first-order CE with the experimental data. When the driving pulse $\eta(t)$ is switched on, the cavity probability amplitude $|\langle a(t) \rangle|^2$ exhibits damped Rabi oscillations and tends towards a stationary value. After switching the driving field off at $t = 0.8\,\mu s$, the Rabi oscillations show up again before the system finally decays to zero. As expected, the dynamics in this regime is well described by the first-order CE and coincides with the results obtained from the Holstein-Primakoff approximation (data not shown). The data presented in Figure 3.6 is the last one out of a series of measurements (where the driving power $|\eta|^2$ was gradually increased) that meets the scalability

criterion $|\langle a(t) \rangle|^2 \propto |\eta|^2$ and thereby marks the end of the linear regime. In the following we will take the driving field amplitude $\eta_0 = \eta/\kappa = 0.2 \cdot 10^6$, which was used in the calculations shown in Figure 3.6, as a reference for the studies in the nonlinear regime beyond $\eta_0$. It is worth noting that the transition from the linear to the nonlinear behaviour is a continuous one and therefore there is some arbitrariness in our choice of $\eta_0$.
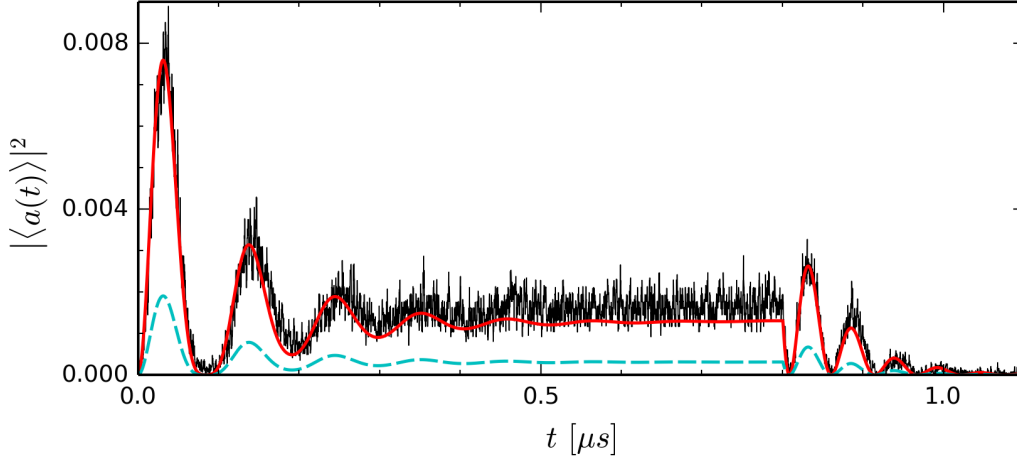


Figure 3.6.: *Linear regime* - Dynamics of the cavity probability amplitude $|\langle a(t) \rangle|^2$ in arbitrary units. The result obtained from the 1st-order CE (*solid red line*) is compared with the experimental data (*black line*). Here the normalized driving field amplitude used in the calculations is $\eta_0 = \eta/\kappa = 0.2 \cdot 10^6$ ($\kappa/2\pi = 0.4$ MHz and $N = 10^{12}$). To illustrate the linearity, we plot additionally the results calculated for a driving field amplitude $\eta_0/2$ (*dashed cyan line*), which gives the same dynamics for $|\langle a(t) \rangle|^2$ but smaller by a factor $1/4$.

**Nonlinear Regime**   If the amplitude of the driving field is further increased, the number of spin excitations in the ensemble becomes significant for the behaviour of the system, which thereby enters the nonlinear regime. Figures 3.7 (a)-(f) provide the experimental data on the transmission through the cavity ($\propto |\langle a(t) \rangle|^2$) for a stepwise increase of the driving power, together with the calculated dynamics employing the Holstein-Primakoff approximation and the first-order CE. It can be seen that in (a), where the incident power was increased by $6 \, \mathrm{dB}$ with respect to the reference driving power $|\eta_0|^2$ (this corresponds approximately to a factor 2 in the amplitude $\eta$), the actual dynamics of the system already starts to deviate from the results predicted by the Holstein-Primakoff approximation. However, the first-order CE accounts for the dynamics of the ensemble in the nonlinear regime very well over nearly $12 \, \mathrm{dB}$. Figures 3.7 (a)-(d), indeed, show a remarkable agreement between our theoretical model and the experimental data.
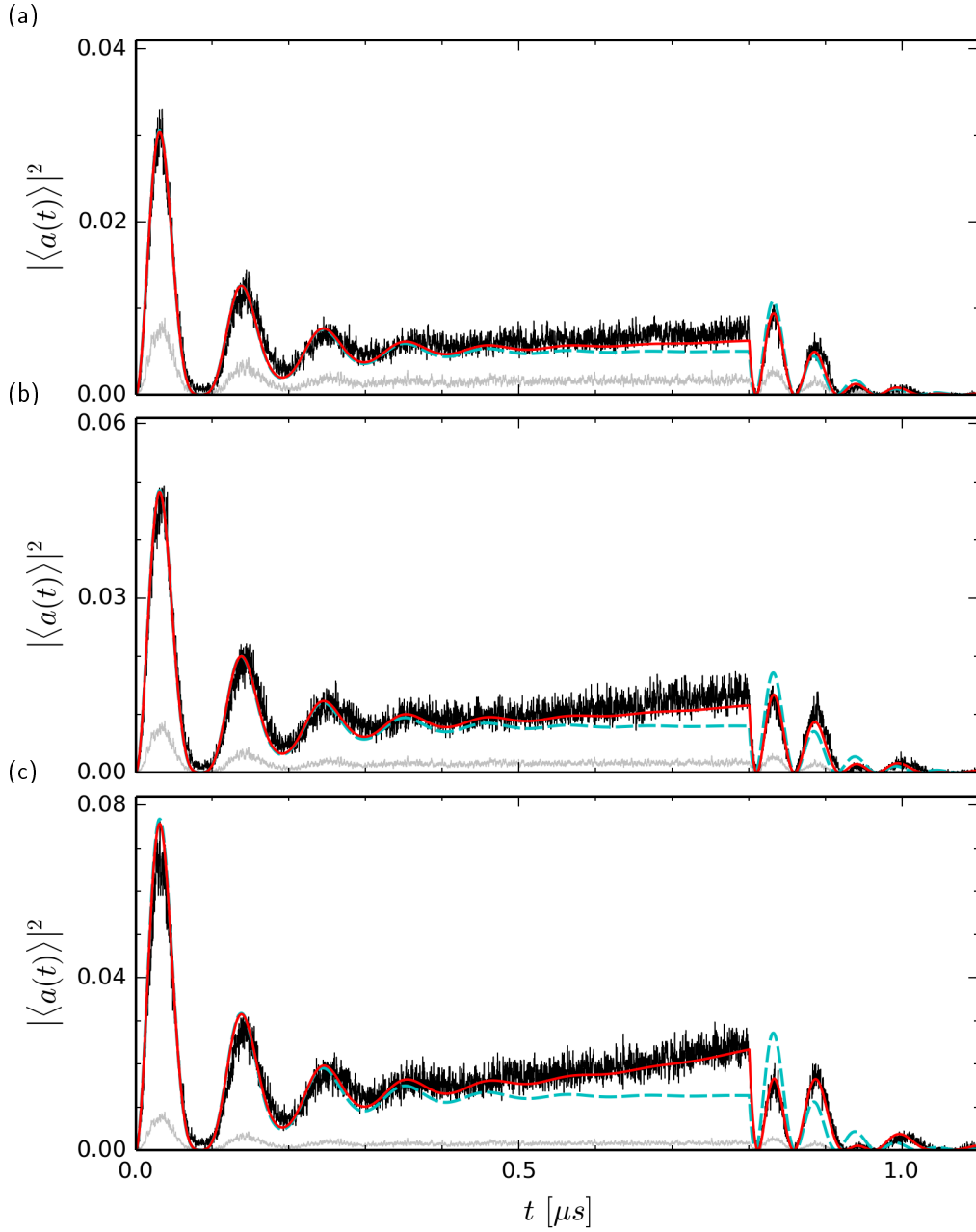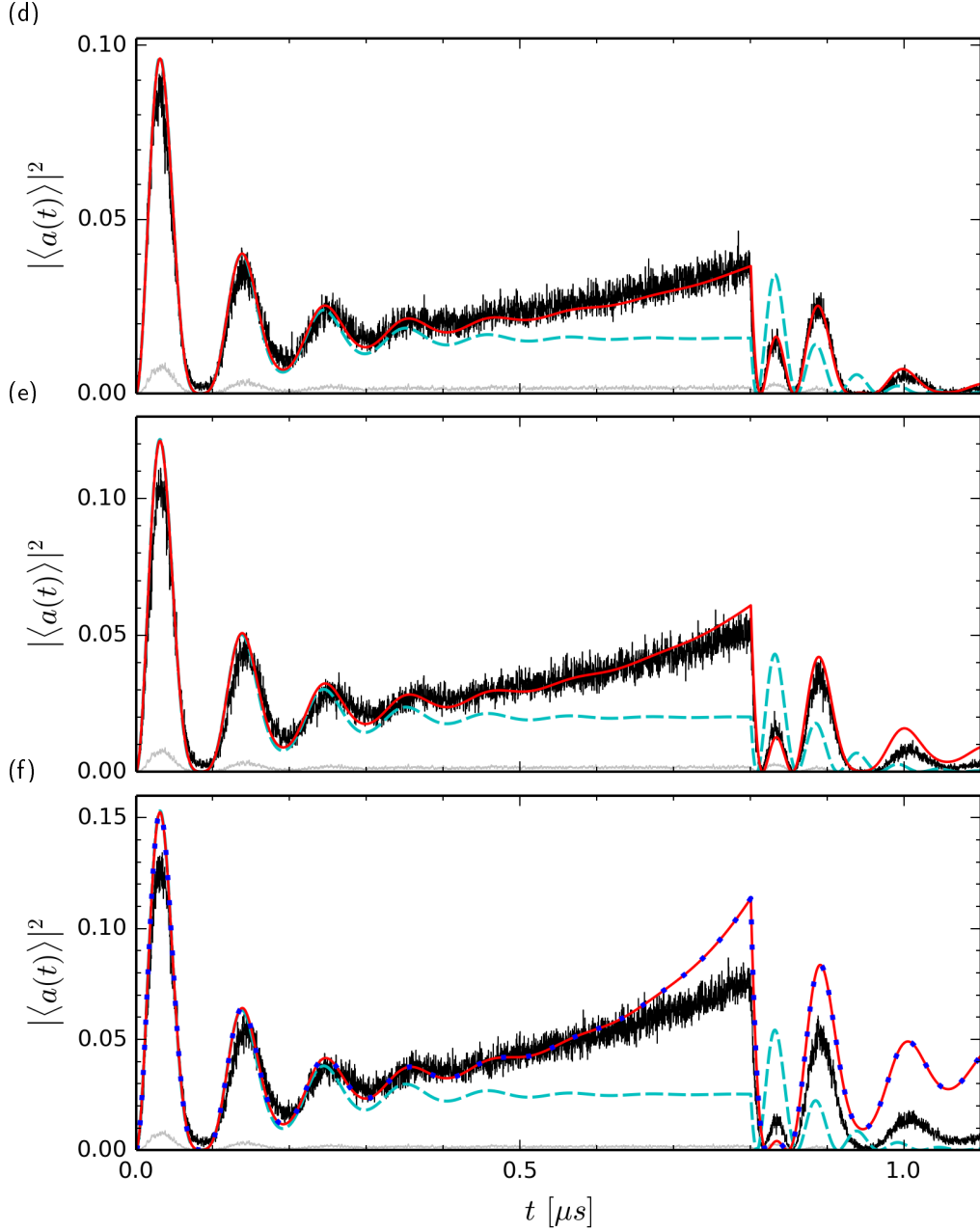
(a)

(b)

(c)



Figure 3.7 (a)-(c).: *Nonlinear regime* - Dynamics of the cavity probability amplitude $|\langle a(t)\rangle|^2$ in arbitrary units. The results obtained from the $1^{\text{st}}$-order CE (*solid red line*) are compared with the experimental data (*black line*). The results obtained from the Holstein-Primakoff approximation are also shown (*dashed cyan line*). In the experiment the incident power was increased by (a) $6\,\text{dB}$, (b) $8\,\text{dB}$, and (c) $10\,\text{dB}$ with respect to the linear reference (*grey line*), which is presented in Figure 3.6 and corresponds to the driving power $|\eta_0|^2$.

Figure 3.7 (d)-(f).: *Nonlinear regime* - Dynamics of the cavity probability amplitude $|\langle a(t)\rangle|^2$ in arbitrary units. The results obtained from the 1$^{\text{st}}$-order CE (*solid red line*) are compared with the experimental data (*black line*). The results obtained from the Holstein-Primakoff approximation are also shown (*dashed cyan line*). In the experiment the incident power was increased by (d) $11\,$dB, (e) $12\,$dB, and (f) $13\,$dB with respect to the linear reference (*grey line*) that is presented in Figure 3.6 and corresponds to the driving power $|\eta_0|^2$. In the last panel (f) we show additionally the results obtained from the 3$^{\text{rd}}$-order CE (*blue dots*), which coincide with those obtained from 1$^{\text{st}}$-order.

For driving powers of $13\,\mathrm{dB}$ with respect to $|\eta_0|^2$, Figure 3.7 (f) indicates that the CE approach overestimates the nonlinear dynamics of the system. Interestingly, for the presented parameter regime, no difference between the first-, second-, and third-order CE is observed. This finding was unexpected and suggests that, in contrast to the case of very few spins, correlations within the large ensemble-cavity system play only a minor role for the investigated driving fields. The fact that the full factorization works so well for a broad range of driving powers might be understood by the vast amount of spins inside the cavity, which results in a declining contribution of the individual spins to the dynamics of the collective cavity mode. Indeed, the influence of strong correlations on the system's behaviour is an important issue for future research.

Our findings suggest that the failure of the CE approach for driving powers beyond $12\,\mathrm{dB}$ with respect to our linear reference $|\eta_0|^2$ can not be related to the formation of correlations within the system but calls for other explanations. It is apparent that the slope of the measured cavity probability amplitude $|\langle a(t) \rangle|^2$ for $t > 0.5\,\mu s$ is much flatter as compared to our calculated values. This discrepancy may be due to an additional loss or dephasing mechanism that is neglected in our model. For instance, it is suggested that our assumption of homogeneous coupling strengths $g_\mu = g$ might not be fulfilled in the experimental realization. Of course, if the cavity field is not homogeneous or the spin ensemble is not well confined inside the cavity, there is some spatial dependence in the coupling strength, which might cause an additional dephasing of the spin ensemble. It should be noted that in principle it is technically possible to include such a spatial dependence of the coupling strength to our model, which is an interesting issue for future studies.

# Chapter 4.

# Conclusions and Outlook

The main goal of this thesis was the development of a theoretical framework that accurately accounts for the nonlinear dynamics of large and inhomogeneously broadened spin ensembles coupled to a single mode cavity. We established such a model by means of an intuitive cumulant expansion approach along with a straightforward clustering procedure.

Our theoretical model was tested for the Tavis-Cummings model with a single spin $N = 1$, which constitutes the well studied Jaynes-Cummings model, and $N = 3$, which additionally allows for spin-spin correlations inside this three-spin system. The results of this investigation show that for both cases the developed cumulant expansion approach is a suitable method to describe the stationary states as well as the temporal evolution of the system even in the nonlinear regime. Our approach, therefore, is applicable for driving powers that are not accessible in the Holstein-Primakoff approximation ($\langle \sigma_k^z(t) \rangle = -1$). Although the first-order cumulant expansion produces considerable deviations from the exact solution given by the quantum master equation for certain parameter regions (mainly for large coupling strengths and driving powers), our results show that one can overcome this problem by the inclusion of higher-order cumulants.

Furthermore, the developed theoretical framework was used to describe the dynamics of a specific physical realization of the driven Tavis-Cummings model based on NV centers in diamond [31–33]. The specific set-up under consideration involved a very large ensemble of $\sim 10^{12}$ spins inhomogeneously broadened in frequency. In previous studies the theoretical description of this system was limited to the linear regime of low driving powers where most spins remain unexcited and the Holstein-Primakoff approximation can be applied. The present investigation shows that the cumulant expansion approach developed in this thesis accurately describes the temporal evolution of the system also for strong driving powers up to almost $12\,\text{dB}$ above the limiting powers of the linear regime. Interestingly, this improvement is achieved even by the first-order cumulant expansion; for the investigated parameter regime there were no significant differences between the solutions obtained from the first-, second-, and third-order cumulant expansion. These findings suggest that the discrepancy arising between our theory and the experimental data for driving

powers with more than $12\,\mathrm{dB}$ above the linear regime can not be related to the formation of correlations within the system. Instead, the deviation of the experimental data from the theoretical predictions might be attributed to a spatial dependence of the cavity-spin couplings $g_k$, which was not considered in the model developed in this thesis. The inclusion of such a dependence into our model is an interesting prospect for future studies. However, at the time of writing this thesis, the group of experimentalists headed by Prof. Jörg Schmiedmayer at the Atominstitut of the Vienna University of Technology puts much effort on improving the experimental set-up in such a way as to ensure a constant coupling strength within the whole ensemble. The new experimental configuration is expected to be in accordance with the developed theoretical model for even stronger driving amplitudes $\eta$. Overall, in this thesis we provide a promising tool for the investigation of interesting nonlinear effects arising in large and inhomogeneously broadened spin ensembles. Specifically our model will serve as a base for future studies dealing with superradiance and superabsorption in connection with inhomogeneous broadening.

# Appendices

# A. Moments and Cumulants

Let us recall the basic definitions of moments and cumulants from statistics and probability theory [48, 49], first for the case of a single random variable and then for the multivariate case.

**Single Random Variable**  Let $p(x)$ be the probability distribution of some stochastic variable $x$. Then the *n-th moment* of $x$ is defined as the expectation value of $x^n$:

$$\langle x^n \rangle := \int_{-\infty}^{\infty} x^n \, p(x) dx \,. \tag{A.1}$$

It is often convenient to introduce the *moment generating function*,

$$M(\xi) := \langle e^{x\xi} \rangle \tag{A.2}$$

where $\xi$ is some real parameter. With the use of this generating function one can write down the $n$-th moment as

$$\langle x^n \rangle = \left[ \frac{d^n M(\xi)}{d\xi^n} \right]_{\xi=0} \,. \tag{A.3}$$

Similarly one can introduce the *cumulant generating function* as the logarithm of the moment generating function $M(\xi)$:

$$K(\xi) := \ln \langle e^{x\xi} \rangle \,, \tag{A.4}$$

which in turn give rise to the *n-th cumulant* of $x$

$$\langle x^n \rangle_c := \left[ \frac{d^n}{d\xi^n} \ln \langle e^{x\xi} \rangle \right]_{\xi=0} \,. \tag{A.5}$$

**Multivariate Case**  For a random vector $\vec{x} = \{x_1, x_2, \ldots\}$ the moment generating function $M(\vec{\xi})$ is defined as follows

$$M(\vec{\xi}) := \langle e^{\xi_1 x_1 + \xi_2 x_2 + \cdots} \rangle \,, \tag{A.6}$$

where $\xi_1, \xi_2, \ldots$ are again real valued parameters. From this definition one can generate the *joint moments* via partial derivatives

$$\langle x_1^{\alpha_1} x_2^{\alpha_2} \ldots \rangle := \left[ \frac{\partial^{\alpha_1 + \alpha_2 + \cdots}}{\partial \xi_1^{\alpha_1} \partial \xi_2^{\alpha_2} \ldots} \langle e^{\xi_1 x_1 + \xi_2 x_2 + \cdots} \rangle \right]_{\xi_i = 0} \,. \tag{A.7}$$

Introducing the cumulant generating function for the random vector $\vec{x}$

$$K(\vec{\xi}) := \ln \langle e^{\xi_1 x_1 + \xi_2 x_2 + \cdots} \rangle \,, \tag{A.8}$$

the *joint cumulant* is given by

$$\langle x_1^{\alpha_1} x_2^{\alpha_2} \ldots \rangle_c := \left[ \frac{\partial^{\alpha_1 + \alpha_2 + \cdots}}{\partial \xi_1^{\alpha_1} \partial \xi_2^{\alpha_2} \ldots} \ln \langle e^{\xi_1 x_1 + \xi_2 x_2 + \cdots} \rangle \right]_{\xi_i = 0} \,. \tag{A.9}$$

# B.  Set of Equations for the Tavis-Cummings Model

Using the generalized Ehrenfest equation (2.3) with the Tavis-Cummings Hamiltonian (2.21) and the Lindblad term (2.22), it is straight forward - although tedious - to derive the following set of equations. Here we present the hierarchy of equations of motion for expectation values up to third order, except of those involving three or more spin operators, as we neglect correlations among them anyway (see Section 2.2.2). Throughout our calculations we use the commutation relations (2.23) as well as $\langle A^{\dagger} \rangle = \langle A \rangle^{*}$, $\langle B^{\dagger} A^{\dagger} \rangle = \langle AB \rangle^{*}$, where the asterisk ($^{*}$) denotes complex conjugation. Note further that all expectation values including multiple operators for the same spin $k$ are reduced by employing the identities $\sigma_k^z \sigma_k^z = \hat{1}$, $\quad \sigma_k^- \sigma_k^- = \hat{0}$, $\quad \sigma_k^z \sigma_k^- = -\sigma_k^-$, $\quad \sigma_k^+ \sigma_k^z = -\sigma_k^+$, $\quad \sigma_k^+ \sigma_k^- = \frac{1}{2}(\hat{1} + \sigma_k^z)$.

$$\frac{d}{dt} \langle a \rangle = -(\kappa + i\,\Delta_c) \langle a \rangle - i \sum_{k=1}^{N} g_k \langle \sigma_k^- \rangle + \eta \tag{B.1}$$

$$\frac{d}{dt} \langle \sigma_k^- \rangle = -(\gamma_h + 2\gamma_p + i\,\Delta_k) \langle \sigma_k^- \rangle + i\,g_k \langle \sigma_k^z a \rangle \tag{B.2}$$

$$\frac{d}{dt} \langle \sigma_k^z \rangle = -2\gamma_h(\langle \sigma_k^z \rangle + 1) + 2i\,g_k( \langle \sigma_k^- a^{\dagger} \rangle - \langle \sigma_k^- a^{\dagger} \rangle^{*} )$$

$$= -2\gamma_h(\langle \sigma_k^z \rangle + 1) - 4\,g_k \,\mathrm{Im}(\langle \sigma_k^- a^{\dagger} \rangle) \tag{B.3}$$

$$\frac{d}{dt} \langle \sigma_k^z a \rangle = -\,(\kappa + 2\gamma_h + i\,\Delta_c) \langle \sigma_k^z a \rangle - 2\gamma_h \langle a \rangle + \eta \langle \sigma_k^z \rangle - i \sum_{\substack{j=1 \\ j \neq k}}^{N} g_j \langle \sigma_k^z \sigma_j^- \rangle$$

$$+ ig_k \langle \sigma_k^- \rangle + 2i\,g_k( \langle \sigma_k^- a^{\dagger} a \rangle - \langle \sigma_k^- a^{\dagger} a^{\dagger} \rangle^{*} ) \tag{B.4}$$

$$\frac{d}{dt} \langle \sigma_k^z \sigma_j^- \rangle \underset{j \neq k}{=} -\,(3\gamma_h + 2\gamma_p + i\,\Delta_j) \langle \sigma_k^z \sigma_j^- \rangle - 2\gamma_h \langle \sigma_j^- \rangle + i\,g_j \langle \sigma_k^z \sigma_j^z a \rangle$$

$$+ 2i\,g_k( \langle \sigma_k^- \sigma_j^- a^{\dagger} \rangle - \langle \sigma_k^+ \sigma_j^- a \rangle ) \tag{B.5}$$

$$\frac{d}{dt} \langle \sigma_k^- a^{\dagger} \rangle = -\,(\kappa + \gamma_h + 2\gamma_p + i\,(\Delta_k - \Delta_c)) \langle \sigma_k^- a^{\dagger} \rangle + \eta \langle \sigma_k^- \rangle + i \sum_{\substack{j=1 \\ j \neq k}}^{N} g_j \langle \sigma_j^+ \sigma_k^- \rangle$$

$$+ i\,\frac{g_k}{2} (\langle \sigma_k^z \rangle + 1) + i\,g_k \langle \sigma_k^z a^{\dagger} a \rangle \tag{B.6}$$

$$\frac{d}{dt} \langle \sigma_k^+ \sigma_j^- \rangle \underset{j \neq k}{=} -\,(2\gamma_h + 4\gamma_p + i\,(\Delta_j - \Delta_k)) \langle \sigma_k^+ \sigma_j^- \rangle - i\,g_k \langle \sigma_k^z \sigma_j^- a^{\dagger} \rangle + i\,g_j \langle \sigma_j^z \sigma_k^- a^{\dagger} \rangle^{*}$$

$$\tag{B.7}$$

$$\frac{d}{dt}\langle\sigma_k^- a\rangle = -\left(\kappa + \gamma_h + 2\gamma_p + i\left(\Delta_k + \Delta_c\right)\right)\langle\sigma_k^- a\rangle + \eta\langle\sigma_k^-\rangle - i\sum_{\substack{j=1\\j\neq k}}^{N}g_j\langle\sigma_k^-\sigma_j^-\rangle$$

$$+ i\,g_k\langle\sigma_k^z aa\rangle \tag{B.8}$$

$$\frac{d}{dt}\langle a^\dagger a^\dagger\rangle = -2(\kappa - i\,\Delta_c)\langle a^\dagger a^\dagger\rangle + 2i\sum_{k=1}^{N}g_k\langle\sigma_k^- a\rangle^* + 2\eta\langle a\rangle^* \tag{B.9}$$

$$\frac{d}{dt}\langle a^\dagger a\rangle = -2\kappa\langle a^\dagger a\rangle - i\sum_{k=1}^{N}g_k(\langle\sigma_k^- a^\dagger\rangle - \langle\sigma_k^- a^\dagger\rangle^*) + \eta\left(\langle a\rangle + \langle a\rangle^*\right)$$

$$= -2\kappa\langle a^\dagger a\rangle + 2\sum_{k=1}^{N}g_k\,\mathrm{Im}(\langle\sigma_k^- a^\dagger\rangle) + 2\eta\,\mathrm{Re}(\langle a\rangle) \tag{B.10}$$

$$\frac{d}{dt}\langle\sigma_k^z\sigma_j^z\rangle \underset{j\neq k}{=} -2\gamma_h(\langle\sigma_k^z\rangle + \langle\sigma_k^z\sigma_j^z\rangle + \langle\sigma_j^z\rangle + \langle\sigma_j^z\sigma_k^z\rangle)$$

$$+ 2i\,g_k(\langle\sigma_j^z\sigma_k^- a^\dagger\rangle - \langle\sigma_j^z\sigma_k^- a^\dagger\rangle^*) + 2i\,g_j(\langle\sigma_k^z\sigma_j^- a^\dagger\rangle - \langle\sigma_k^z\sigma_j^- a^\dagger\rangle^*)$$

$$= -2\gamma_h(\langle\sigma_k^z\rangle + \langle\sigma_k^z\sigma_j^z\rangle + \langle\sigma_j^z\rangle + \langle\sigma_j^z\sigma_k^z\rangle)$$

$$- 4g_k\,\mathrm{Im}(\langle\sigma_j^z\sigma_k^- a^\dagger\rangle) - 4g_j\,\mathrm{Im}(\langle\sigma_k^z\sigma_j^- a^\dagger\rangle) \tag{B.11}$$

$$\frac{d}{dt}\langle\sigma_k^-\sigma_j^-\rangle \underset{j\neq k}{=} -(2\gamma_h + 4\gamma_p + i\left(\Delta_j + \Delta_k\right))\langle\sigma_k^-\sigma_j^-\rangle + i\,g_k\langle\sigma_k^z\sigma_j^- a\rangle + i\,g_j\langle\sigma_j^z\sigma_k^- a\rangle \tag{B.12}$$

$$\frac{d}{dt}\langle\sigma_k^z a^\dagger a\rangle = -2(\kappa + \gamma_h)\langle\sigma_k^z a^\dagger a\rangle - 2\gamma_h\langle a^\dagger a\rangle + \eta(\langle\sigma_k^z a\rangle + \langle\sigma_k^z a\rangle^*)$$

$$- i\sum_{\substack{j=1\\j\neq k}}^{N}g_j(\langle\sigma_k^z\sigma_j^- a^\dagger\rangle - \langle\sigma_k^z\sigma_j^- a^\dagger\rangle^*) + i\,g_k(\langle\sigma_k^- a^\dagger\rangle - \langle\sigma_k^- a^\dagger\rangle^*)$$

$$+ 2i\,g_k(\langle\sigma_k^- a^\dagger a^\dagger a\rangle - \langle\sigma_k^- a^\dagger a^\dagger a\rangle^*)$$

$$= -2(\kappa + \gamma_h)\langle\sigma_k^z a^\dagger a\rangle - 2\gamma_h\langle a^\dagger a\rangle + 2\eta\,\mathrm{Re}(\langle\sigma_k^z a\rangle) - 2\,g_k\,\mathrm{Im}(\langle\sigma_k^- a^\dagger\rangle)$$

$$+ 2\sum_{\substack{j=1\\j\neq k}}^{N}g_j\,\mathrm{Im}(\langle\sigma_k^z\sigma_j^- a^\dagger\rangle) - 4\,g_k\,\mathrm{Im}(\langle\sigma_k^- a^\dagger a^\dagger a\rangle) \tag{B.13}$$

$$\frac{d}{dt}\langle\sigma_k^- a^\dagger a\rangle = -\left(2(\kappa + \gamma_p) + \gamma_h + i\Delta_k\right)\langle\sigma_k^- a^\dagger a\rangle + \eta(\langle\sigma_k^- a^\dagger\rangle + \langle\sigma_k^- a\rangle) + i\,g_k\langle\sigma_k^z a^\dagger aa\rangle$$

$$+ i\sum_{\substack{j=1\\j\neq k}}^{N}g_j(\langle\sigma_j^+\sigma_k^- a\rangle - \langle\sigma_k^-\sigma_j^- a^\dagger\rangle) + i\frac{g_k}{2}(\langle\sigma_k^z a\rangle + \langle a\rangle) \tag{B.14}$$

$$\frac{d}{dt} \langle \sigma_k^- a^\dagger a^\dagger \rangle = - \left( 2(\kappa + \gamma_p) + \gamma_h + i(\Delta_k - 2\Delta_c) \right) \langle \sigma_k^- a^\dagger a^\dagger \rangle + 2\eta \langle \sigma_k^- a^\dagger \rangle$$

$$+ 2i \sum_{\substack{j=1 \\ j \neq k}}^{N} g_j \langle \sigma_j^+ \sigma_k^- a^\dagger \rangle + i \, g_k (\langle \sigma_k^z a \rangle^* + \langle a \rangle^*) + i \, g_k \langle \sigma_k^z a^\dagger a^\dagger a \rangle \qquad \text{(B.15)}$$

$$\frac{d}{dt} \langle \sigma_k^z a a \rangle = - 2(\kappa + \gamma_h + i\Delta_c) \langle \sigma_k^z a a \rangle - 2\gamma_h \langle a^\dagger a^\dagger \rangle^* + 2\eta \langle \sigma_k^z a \rangle + 2i \, g_k \langle \sigma_k^- a \rangle$$

$$- 2i \sum_{\substack{j=1 \\ j \neq k}}^{N} g_j \langle \sigma_k^z \sigma_j^- a \rangle + 2i \, g_k (\langle \sigma_k^- a^\dagger a a \rangle - \langle \sigma_k^+ a a a \rangle) \qquad \text{(B.16)}$$

$$\frac{d}{dt} \langle \sigma_k^- a a \rangle = - \left( 2(\kappa + \gamma_p) + \gamma_h + i(\Delta_k + 2\Delta_c) \right) \langle \sigma_k^- a a \rangle + 2\eta \langle \sigma_k^- a \rangle$$

$$- 2i \sum_{\substack{j=1 \\ j \neq k}}^{N} g_j \langle \sigma_k^- \sigma_j^- a \rangle + i \, g_k \langle \sigma_k^z a a a \rangle \qquad \text{(B.17)}$$

$$\frac{d}{dt} \langle a^\dagger a a \rangle = - (3\kappa + i \, \Delta_c) \langle a^\dagger a a \rangle - 2i \sum_{k=1}^{N} g_k \langle \sigma_k^- a^\dagger a \rangle + i \sum_{k=1}^{N} g_k \langle \sigma_k^- a^\dagger a^\dagger \rangle^*$$

$$+ 2\eta \langle a^\dagger a \rangle + \eta \langle a^\dagger a^\dagger \rangle^* \qquad \text{(B.18)}$$

$$\frac{d}{dt} \langle a a a \rangle = - 3(\kappa + i \, \Delta_c) \langle a a a \rangle - 3i \sum_{k=1}^{N} g_k \langle \sigma_k^- a a \rangle + 3\eta \langle a^\dagger a^\dagger \rangle^* \qquad \text{(B.19)}$$

$$\frac{d}{dt} \langle \sigma_k^z \sigma_j^z a \rangle \underset{j \neq k}{=} - (\kappa + i\Delta_c) \langle \sigma_k^z \sigma_j^z a \rangle - 2\gamma_h (\langle \sigma_k^z a \rangle + \langle \sigma_k^z \sigma_j^z a \rangle + \langle \sigma_j^z a \rangle + \langle \sigma_j^z \sigma_k^z a \rangle)$$

$$+ 2i(g_k \langle \sigma_j^z \sigma_k^- a^\dagger a \rangle + g_j \langle \sigma_k^z \sigma_j^- a^\dagger a \rangle - g_k \langle \sigma_j^z \sigma_k^+ a a \rangle - g_j \langle \sigma_k^z \sigma_j^+ a a \rangle)$$

$$- i \sum_{\substack{m=1 \\ m \neq k,j}}^{N} g_m \langle \sigma_k^z \sigma_j^z \sigma_m^- \rangle + i \, g_k \langle \sigma_j^z \sigma_k^- \rangle + i \, g_j \langle \sigma_k^z \sigma_j^- \rangle \qquad \text{(B.20)}$$

$$\frac{d}{dt} \langle \sigma_k^- \sigma_j^- a^\dagger \rangle \underset{j \neq k}{=} - (\kappa + 2\gamma_h + 4\gamma_p + i(\Delta_k + \Delta_j - \Delta_c)) \langle \sigma_k^- \sigma_j^- a^\dagger \rangle + \eta \langle \sigma_k^- \sigma_j^- \rangle$$

$$+ i \sum_{\substack{m=1 \\ m \neq k,j}}^{N} g_m \langle \sigma_m^+ \sigma_k^- \sigma_j^- \rangle + i\frac{g_k}{2}(\langle \sigma_j^- \rangle + \langle \sigma_k^z \sigma_j^- \rangle) + i\frac{g_j}{2}(\langle \sigma_k^- \rangle + \langle \sigma_j^z \sigma_k^- \rangle)$$

$$+ i \, g_k \langle \sigma_k^z \sigma_j^- a^\dagger a \rangle + i \, g_j \langle \sigma_j^z \sigma_k^- a^\dagger a \rangle \qquad \text{(B.21)}$$

$$\frac{d}{dt}\left\langle\sigma_k^+\sigma_j^-a\right\rangle \underset{j\neq k}{=} -\left(\kappa+2\gamma_h+4\gamma_p+i(\Delta_j-\Delta_k+\Delta_c)\right)\left\langle\sigma_k^+\sigma_j^-a\right\rangle+\eta\left\langle\sigma_k^+\sigma_j^-\right\rangle$$

$$-i\sum_{\substack{m=1\\m\neq k,j}}^{N}g_m\left\langle\sigma_k^+\sigma_j^-\sigma_m^-\right\rangle-i\frac{g_k}{2}(\left\langle\sigma_j^-\right\rangle+\left\langle\sigma_k^z\sigma_j^-\right\rangle)$$

$$-i\,g_k\left\langle\sigma_k^z\sigma_j^-a^\dagger a\right\rangle+i\,g_j\left\langle\sigma_k^+\sigma_j^z aa\right\rangle \tag{B.22}$$

$$\frac{d}{dt}\left\langle\sigma_k^z\sigma_j^-a^\dagger\right\rangle \underset{j\neq k}{=} -\left(\kappa+3\gamma_h+2\gamma_p+i(\Delta_j-\Delta_c)\right)\left\langle\sigma_k^z\sigma_j^-a^\dagger\right\rangle-2\gamma_h\left\langle\sigma_j^-a^\dagger\right\rangle+\eta\left\langle\sigma_k^z\sigma_j^-\right\rangle$$

$$+i\sum_{\substack{m=1\\m\neq k,j}}^{N}g_m\left\langle\sigma_m^+\sigma_k^z\sigma_j^-\right\rangle-i\,g_k\left\langle\sigma_k^+\sigma_j^-\right\rangle+i\frac{g_j}{2}(\left\langle\sigma_k^z\right\rangle+\left\langle\sigma_k^z\sigma_j^z\right\rangle)$$

$$+i\,g_j\left\langle\sigma_k^z\sigma_j^z a^\dagger a\right\rangle+2i\,g_k(\left\langle\sigma_k^-\sigma_j^-a^\dagger a^\dagger\right\rangle-\left\langle\sigma_k^+\sigma_j^-a^\dagger a\right\rangle) \tag{B.23}$$

$$\frac{d}{dt}\left\langle\sigma_k^z\sigma_j^-a\right\rangle \underset{j\neq k}{=} -\left(\kappa+3\gamma_h+2\gamma_p+i(\Delta_j+\Delta_c)\right)\left\langle\sigma_k^z\sigma_j^-a\right\rangle-2\gamma_h\left\langle\sigma_j^-a\right\rangle+\eta\left\langle\sigma_k^z\sigma_j^-\right\rangle$$

$$-i\sum_{\substack{m=1\\m\neq k,j}}^{N}g_m\left\langle\sigma_k^z\sigma_j^-\sigma_m^-\right\rangle+i\,g_k\left\langle\sigma_k^-\sigma_j^-\right\rangle+i\,g_j\left\langle\sigma_k^z\sigma_j^z aa\right\rangle$$

$$+2i\,g_k(\left\langle\sigma_k^-\sigma_j^-a^\dagger a\right\rangle-\left\langle\sigma_k^+\sigma_j^-aa\right\rangle) \tag{B.24}$$

$$\frac{d}{dt}\left\langle\sigma_k^-\sigma_j^-a\right\rangle \underset{j\neq k}{=} -\left(\kappa+2\gamma_h+4\gamma_p+i(\Delta_k+\Delta_j+\Delta_c)\right)\left\langle\sigma_k^-\sigma_j^-a\right\rangle+\eta\left\langle\sigma_k^-\sigma_j^-\right\rangle$$

$$-i\sum_{\substack{m=1\\m\neq k,j}}^{N}g_m\left\langle\sigma_k^-\sigma_j^-\sigma_m^-\right\rangle+i\,g_k\left\langle\sigma_k^z\sigma_j^- aa\right\rangle+i\,g_j\left\langle\sigma_j^z\sigma_k^- aa\right\rangle \tag{B.25}$$

# C.  Nitrogen-Vacancy Ensemble in Diamond

In this appendix we focus on a particular experimental realization for the driven Tavis-Cummings model based on the negatively charged nitrogen vacancy (NV) centers in diamond, which constitute a very promising physical system for emergent quantum technologies, with a broad range of possible applications [59]. In particular the NV centers show great potential for the storage of quantum information, owing to their long coherence times (up to one second [60] for a single NV) and to the combination of microwave and optical transitions which makes them an easily accessible and controllable qubit [61]. The coupling between a single NV center and an electromagnetic field is typically rather weak $\sim 10\,\text{Hz}$; however, for an ensemble of N spins the collective coupling is enhanced by a factor $\sqrt{N}$, which allows to reach the strong coupling regime that is required for quantum information processing [18]. Such an ensemble of NV centers is naturally imposed to an inhomogeneous broadening of the transition frequencies $\omega_k$, mainly due to local dipole-dipole coupling of the NV centers to other magnetic impurities inside the diamond. In accordance with previous studies [19, 31–33] this line broadening is well described by taking a $q$-Gaussian distribution function [62] for the spectral spin density

$$\rho(\omega) = C \left[ 1 - (1-q)\frac{(\omega - \omega_s)^2}{\Delta^2} \right]^{\frac{1}{1-q}} , \qquad (C.1)$$
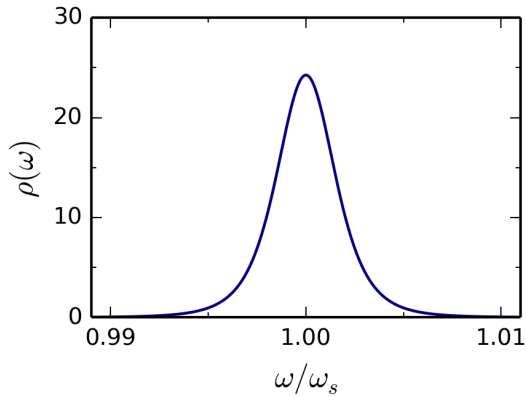


Figure C.1.: The normalized spectral spin distribution $\rho(\omega)$ defined by the $q$-Gaussian distribution function Eq. (C.1) with $q = 1.39$ and $\gamma_q/2\pi = 9.4\,\text{MHz}$.

where $q$ is the dimensionless shape parameter, $\gamma_q := 2\Delta\sqrt{\frac{2^q-2}{2q-2}}$ is the full width at half maximum, and $C$ is the normalization constant. As in the previous studies, for our calculations we use the parameters $q = 1.39$ and $\gamma_q/2\pi = 9.4\,\text{MHz}$. Note that this spin distribution, which is presented in Figure C.1, is situated between a Gaussian ($q \to 1$) and a Lorentzian ($q = 2$) distribution.

In the experiment, which was performed at the Atominstitut of the Vienna University of Technology, the NV ensemble is magnetically coupled to a $\lambda/2$ superconducting microwave coplanar waveguide resonator. The experiment is carried out in a standard dilution refrigerator with a synthetic diamond placed on top of a resonator. In order to avoid thermal excitations the set-up is cooled to a temperature of $\sim 25\,\text{mK}$. The

NV ensemble is Zeeman tuned into resonance with the cavity frequency $\omega_c/2\pi = 2.6915\,\text{GHz}$ by a set of superconducting Helmholtz coils. To probe the cavity-spin system, a time-resolved transmission spectroscopy is performed by a fast homodyne detection set-up with subnanosecond time resolution (see [31] for more details).

# Acknowledgements

# Bibliography

[1] R. P. Feynman, *QED: The Strange Theory of Light and Matter.* 1988.

[2] E. M. Purcell, "Spontaneous emission probabilities at radio frequencies," *Phys. Rev.*, vol. 69, pp. 674–674, Jun 1946.

[3] P. Goy, J. M. Raimond, M. Gross, and S. Haroche, "Observation of cavity-enhanced single-atom spontaneous emission," *Phys. Rev. Lett.*, vol. 50, pp. 1903–1906, Jun 1983.

[4] R. G. Hulet, E. S. Hilfer, and D. Kleppner, "Inhibited spontaneous emission by a rydberg atom," *Phys. Rev. Lett.*, vol. 55, pp. 2137–2140, Nov 1985.

[5] Y. Kaluzny, P. Goy, M. Gross, J. M. Raimond, and S. Haroche, "Observation of self-induced rabi oscillations in two-level atoms excited inside a resonant cavity: The ringing regime of superradiance," *Phys. Rev. Lett.*, vol. 51, pp. 1175–1178, Sep 1983.

[6] E. T. Jaynes and F. W. Cummings, "Comparison of quantum and semiclassical radiation theories with application to the beam maser," *Proceedings of the IEEE*, vol. 51, pp. 89–109, Jan 1963.

[7] J. H. Eberly, N. B. Narozhny, and J. J. Sanchez-Mondragon, "Periodic spontaneous collapse and revival in a simple quantum model," *Phys. Rev. Lett.*, vol. 44, pp. 1323–1326, May 1980.

[8] R. J. Thompson, G. Rempe, and H. J. Kimble, "Observation of normal-mode splitting for an atom in an optical cavity," *Phys. Rev. Lett.*, vol. 68, pp. 1132–1135, Feb 1992.

[9] C. M. Savage and H. J. Carmichael, "Single atom optical bistability," *IEEE Journal of Quantum Electronics*, vol. 24, pp. 1495–1498, Aug 1988.

[10] H. J. Carmichael, R. J. Brecha, M. G. Raizen, H. J. Kimble, and P. R. Rice, "Subnatural linewidth averaging for coupled atomic and cavity-mode oscillators," *Phys. Rev. A*, vol. 40, pp. 5516–5519, Nov 1989.

[11] B. T. H. Varcoe, S. Brattke, M. Weidinger, and H. Walther, "Preparing pure photon number states of the radiation field," *Nature*, vol. 403, pp. 743–746, Feb. 2000.

[12] A. Rauschenbeutel, G. Nogues, S. Osnaghi, P. Bertet, M. Brune, J. M. Rai-mond, and S. Haroche, "Coherent operation of a tunable quantum phase gate in cavity qed," *Phys. Rev. Lett.*, vol. 83, pp. 5166–5169, Dec 1999.

[13] P. W. Anderson, "More is different," *Science*, vol. 177, no. 4047, pp. 393–396, 1972.

[14] R. H. Dicke, "Coherence in spontaneous radiation processes," *Phys. Rev.*, vol. 93, pp. 99–110, Jan 1954.

[15] R. Bonifacio and L. Lugiato, *Dissipative systems in quantum optics: resonance fluorescence, optical bistability, superfluorescence.* Topics in current physics, Springer-Verlag, 1982.

[16] M. Tavis and F. W. Cummings, "Exact solution for an $n$-molecule—radiation-field hamiltonian," *Phys. Rev.*, vol. 170, pp. 379–384, Jun 1968.

[17] P. Rabl, D. DeMille, J. M. Doyle, M. D. Lukin, R. J. Schoelkopf, and P. Zoller, "Hybrid quantum processors: Molecular ensembles as quantum memory for solid state circuits," *Phys. Rev. Lett.*, vol. 97, p. 033003, Jul 2006.

[18] R. Amsüss, C. Koller, T. Nöbauer, S. Putz, S. Rotter, K. Sandner, S. Schneider, M. Schramböck, G. Steinhauser, H. Ritsch, J. Schmiedmayer, and J. Majer, "Cavity qed with magnetically coupled collective spin states," *Phys. Rev. Lett.*, vol. 107, p. 060502, Aug 2011.

[19] K. Sandner, H. Ritsch, R. Amsüss, C. Koller, T. Nöbauer, S. Putz, J. Schmied-mayer, and J. Majer, "Strong magnetic coupling of an inhomogeneous nitrogen-vacancy ensemble to a cavity," *Phys. Rev. A*, vol. 85, p. 053806, May 2012.

[20] Y. Kubo, F. R. Ong, P. Bertet, D. Vion, V. Jacques, D. Zheng, A. Dréau, J.-F. Roch, A. Auffeves, F. Jelezko, J. Wrachtrup, M. F. Barthe, P. Bergonzo, and D. Esteve, "Strong coupling of a spin ensemble to a superconducting resonator," *Phys. Rev. Lett.*, vol. 105, p. 140502, Sep 2010.

[21] Y. Kubo, C. Grezes, A. Dewes, T. Umeda, J. Isoya, H. Sumiya, N. Morishita, H. Abe, S. Onoda, T. Ohshima, V. Jacques, A. Dréau, J.-F. Roch, I. Diniz, A. Auffeves, D. Vion, D. Esteve, and P. Bertet, "Hybrid quantum circuit with a superconducting qubit coupled to a spin ensemble," *Phys. Rev. Lett.*, vol. 107, p. 220501, Nov 2011.

[22] Y. Kubo, I. Diniz, A. Dewes, V. Jacques, A. Dréau, J.-F. Roch, A. Auffeves, D. Vion, D. Esteve, and P. Bertet, "Storage and retrieval of a microwave field in a spin ensemble," *Phys. Rev. A*, vol. 85, p. 012333, Jan 2012.

[23] S. Probst, H. Rotzinger, S. Wünsch, P. Jung, M. Jerger, M. Siegel, A. V. Ustinov, and P. A. Bushev, "Anisotropic rare-earth spin ensemble strongly coupled to a superconducting resonator," *Phys. Rev. Lett.*, vol. 110, p. 157001, Apr 2013.

[24] J. Verdú, H. Zoubi, C. Koller, J. Majer, H. Ritsch, and J. Schmiedmayer, "Strong magnetic coupling of an ultracold gas to a superconducting waveguide cavity," *Phys. Rev. Lett.*, vol. 103, p. 043603, Jul 2009.

[25] A. Imamoğlu, "Cavity qed based on collective magnetic dipole coupling: Spin ensembles as hybrid two-level systems," *Phys. Rev. Lett.*, vol. 102, p. 083602, Feb 2009.

[26] H. Huebl, C. W. Zollitsch, J. Lotze, F. Hocke, M. Greifenstein, A. Marx, R. Gross, and S. T. B. Goennenwein, "High cooperativity in coupled microwave resonator ferrimagnetic insulator hybrids," *Phys. Rev. Lett.*, vol. 111, p. 127003, Sep 2013.

[27] Y. Tabuchi, S. Ishino, T. Ishikawa, R. Yamazaki, K. Usami, and Y. Nakamura, "Hybridizing ferromagnetic magnons and microwave photons in the quantum limit," *Phys. Rev. Lett.*, vol. 113, p. 083603, Aug 2014.

[28] C. Simon, M. Afzelius, J. Appel, A. Boyer de la Giroday, J. S. Dewhurst, N. Gisin, Y. C. Hu, F. Jelezko, S. Kröll, H. J. Müller, J. Nunn, S. E. Polzik, G. J. Rarity, H. De Riedmatten, W. Rosenfeld, J. A. Shields, N. Sköld, M. R. Stevenson, R. Thew, A. I. Walmsley, C. M. Weber, H. Weinfurter, J. Wrachtrup, and J. R. Young, "Quantum memories," *The European Physical Journal D*, vol. 58, no. 1, pp. 1–22, 2010.

[29] Z.-L. Xiang, S. Ashhab, J. Q. You, and F. Nori, "Hybrid quantum circuits: Superconducting circuits interacting with other quantum systems," *Rev. Mod. Phys.*, vol. 85, pp. 623–653, Apr 2013.

[30] H. Primakoff and T. Holstein, "Many-body interactions in atomic and nuclear systems," *Phys. Rev.*, vol. 55, pp. 1218–1234, Jun 1939.

[31] S. Putz, D. O. Krimer, R. Amsuss, A. Valookaran, T. Nobauer, J. Schmiedmayer, S. Rotter, and J. Majer, "Protecting a spin ensemble against decoherence in the strong-coupling regime of cavity qed," *Nat Phys*, vol. 10, pp. 720–724, Oct. 2014.

[32] D. O. Krimer, S. Putz, J. Majer, and S. Rotter, "Non-markovian dynamics of a single-mode cavity strongly coupled to an inhomogeneously broadened spin ensemble," *Phys. Rev. A*, vol. 90, p. 043852, Oct 2014.

[33]  D. O. Krimer, B. Hartl, and S. Rotter, "Hybrid quantum systems with collectively coupled spin states: Suppression of decoherence through spectral hole burning," *Phys. Rev. Lett.*, vol. 115, p. 033601, Jul 2015.

[34]  H. A. M. Leymann, A. Foerster, and J. Wiersig, "Expectation value based equation-of-motion approach for open quantum systems: A general formalism," *Phys. Rev. B*, vol. 89, p. 085308, Feb 2014.

[35]  M. Kira and S. W. Koch, "Cluster-expansion representation in quantum optics," *Phys. Rev. A*, vol. 78, p. 022102, Aug 2008.

[36]  J. Wiersig, C. Gies, F. Jahnke, M. Aszmann, T. Berstermann, M. Bayer, C. Kistner, S. Reitzenstein, C. Schneider, S. Hofling, A. Forchel, C. Kruse, J. Kalden, and D. Hommel, "Direct observation of correlations between individual photon emission events of a microcavity laser," *Nature*, vol. 460, pp. 245–249, July 2009.

[37]  M. Kira, F. Jahnke, W. Hoyer, and S. Koch, "Quantum theory of spontaneous emission and coherent effects in semiconductor microstructures," *Progress in Quantum Electronics*, vol. 23, no. 6, pp. 189 – 279, 1999.

[38]  R. Kubo, "Generalized cumulant expansion method," *Journal of the Physical Society of Japan*, vol. 17, no. 7, pp. 1100–1120, 1962.

[39]  K. D. B. Higgins, S. C. Benjamin, T. M. Stace, G. J. Milburn, B. W. Lovett, and E. M. Gauger, "Superabsorption of light via quantum engineering," *Nature Communications*, vol. 5, pp. 4705–, Aug. 2014.

[40]  H. Carmichael, *An Open Systems Approach to Quantum Optics: Lectures Presented at the Université Libre de Bruxelles, October 28 to November 4, 1991.* Springer Berlin Heidelberg, 1993.

[41]  H. P. Breuer and F. Petruccione, *The theory of open quantum systems.* Oxford University Press, 2002.

[42]  S. Haroche and J. M. Raimond, *Exploring the Quantum: Atoms, Cavities, and Photons.* Oxford Univ. Press, 2006.

[43]  A. Carmele, M. Richter, W. W. Chow, and A. Knorr, "Antibunching of thermal radiation by a room-temperature phonon bath: A numerically solvable model for a strongly interacting light-matter-reservoir system," *Phys. Rev. Lett.*, vol. 104, p. 156801, Apr 2010.

[44]  J. Kabuss, A. Carmele, T. Brandes, and A. Knorr, "Optically driven quantum dots as source of coherent cavity phonons: A proposal for a phonon laser scheme," *Phys. Rev. Lett.*, vol. 109, p. 054301, Jul 2012.

[45] S. Krämer and H. Ritsch, "Generalized mean-field approach to simulate the dynamics of large open spin ensembles with long range interactions," *The European Physical Journal D*, vol. 69, no. 12, pp. 1–11, 2015.

[46] M. Bonitz, *Quantum Kinetic Theory*. Springer International Publishing, 2015.

[47] M. Scully and M. Zubairy, *Quantum Optics*. Cambridge University Press, 1997.

[48] K. Riley, M. Hobson, and S. Bence, *Mathematical Methods for Physics and Engineering: A Comprehensive Guide*. Cambridge University Press, 2006.

[49] L. Mandel and E. Wolf, *Optical Coherence and Quantum Optics*. Cambridge University Press, 1995.

[50] P. Fulde, *Electron correlations in molecules and solids*. Springer series in solid-state sciences, Springer-Verlag, 1991.

[51] L. E. Ballentine, "Probability theory in quantum mechanics," *American Journal of Physics*, vol. 54, no. 10, pp. 883–889, 1986.

[52] C. W. Gardiner and M. J. Collett, "Input and output in damped quantum systems: Quantum stochastic differential equations and the master equation," *Phys. Rev. A*, vol. 31, pp. 3761–3774, Jun 1985.

[53] G. Agarwal, *Quantum Optics*. Quantum Optics, Cambridge University Press, 2013.

[54] W. H. Press, S. A. Teukolsky, W. T. Vetterling, and B. P. Flannery, *Numerical Recipes 3rd Edition: The Art of Scientific Computing*. New York, NY, USA: Cambridge University Press, 3 ed., 2007.

[55] M. J. D. Powell, "A hybrid method for nonlinear equations," in *Numerical Methods for Nonlinear Algebraic Equations*, P. Rabinowitz (Ed.) 1970.

[56] The direct integration of the master equation for the case $N = 1$ and $N = 3$ is performed using the master equation solver provided by the open-source software package QuTiP (http://qutip.org/). After defining an appropriate Fock-basis for the cavity mode as well as the basis states for the spin operators, the master equation (2.1) is integrated numerically taking into account the full quantum dynamics [57, 58].

[57] J. Johansson, P. Nation, and F. Nori, "Qutip: An open-source python framework for the dynamics of open quantum systems," *Computer Physics Communications*, vol. 183, no. 8, pp. 1760 – 1772, 2012.

[58] J. Johansson, P. Nation, and F. Nori, "Qutip 2: A python framework for the dynamics of open quantum systems," *Computer Physics Communications*, vol. 184, no. 4, pp. 1234 – 1240, 2013.

[59] M. W. Doherty, N. B. Manson, P. Delaney, F. Jelezko, J. Wrachtrup, and L. C. Hollenberg, "The nitrogen-vacancy colour centre in diamond," *Physics Reports*, vol. 528, no. 1, pp. 1 – 45, 2013.

[60] N. Bar-Gill, L. Pham, A. Jarmola, D. Budker, and R. Walsworth, "Solid-state electronic spin coherence time approaching one second," *Nat Commun*, vol. 4, pp. 1743–, Apr. 2013.

[61] L. Childress, M. V. G. Dutt, J. M. Taylor, A. S. Zibrov, F. Jelezko, J. Wrachtrup, P. R. Hemmer, and M. D. Lukin, "Coherent dynamics of coupled electron and nuclear spin qubits in diamond," *Science*, 2006.

[62] C. Tsallis, *Introduction to Nonextensive Statistical Mechanics: Approaching a Complex World.* Springer New York, 2009.